applied sciences

Review

Fabrication of Smart Materials Using Laser Processing: Analysis and Prospects

Serguei P. Murzin [1,2,*] and Christian Stiglbrunner [1]

1 TU Wien, Karlsplatz 13, 1040 Vienna, Austria; christian.stiglbrunner@tuwien.ac.at
2 Samara National Research University, Moskovskoe Shosse 34, Samara 443086, Russia
* Correspondence: serguei.murzin@tuwien.ac.at or murzin@ssau.ru

Abstract: Laser processing is a versatile tool that enhances smart materials for diverse industries, allowing precise changes in material properties and customization of surface characteristics. It drives the development of smart materials with adaptive properties through laser modification, utilizing photothermal reactions and functional additives for meticulous control. These laser-processed smart materials form the foundation of 4D printing that enables dynamic shape changes depending on external influences, with significant potential in the aerospace, robotics, health care, electronics, and automotive sectors, thus fostering innovation. Laser processing also advances photonics and optoelectronics, facilitating precise control over optical properties and promoting responsive device development for various applications. The application of computer-generated diffractive optical elements (DOEs) enhances laser precision, allowing for predetermined temperature distribution and showcasing substantial promise in enhancing smart material properties. This comprehensive overview explores the applications of laser technology and nanotechnology involving DOEs, underscoring their transformative potential in the realms of photonics and optoelectronics. The growing potential for further research and practical applications in this field suggests promising prospects in the near future.

Keywords: smart materials; laser processing; modification; material properties; functional additive introduction; shape memory; 4D printing; optical system; computer-generated diffractive optical elements

Citation: Murzin, S.P.; Stiglbrunner, C. Fabrication of Smart Materials Using Laser Processing: Analysis and Prospects. *Appl. Sci.* **2024**, *14*, 85. https://doi.org/10.3390/app14010085

Academic Editor: Guijun Bi

Received: 27 November 2023
Revised: 16 December 2023
Accepted: 19 December 2023
Published: 21 December 2023

1. Introduction

Smart materials, alternatively referred to as intelligent materials or materials with adaptive properties, constitute a fascinating class of materials endowed with the capability to respond dynamically to changing environmental conditions. These materials exhibit distinctive properties that empower them to undergo adjustments in their physical or chemical structure when subjected to external stimuli. Among the impressive array of smart materials, shape memory materials [1–4] stand out, with their unique ability to "remember" and seamlessly revert to their original shape after deformation. Applications of these materials span a wide spectrum, from medical implants to the aerospace industry. Magnetic shape memory materials [5–7] demonstrate a distinctive characteristic of changing shape under the influence of a magnetic field, making them highly relevant in microelectronics and other innovative applications. Thermoresponsive materials [8–10], which adapt their properties in response to temperature fluctuations, have found applications in a wide range of fields, including medicine, biotechnology, and optoelectronics. Electroactive polymers [11,12], on the other hand, exhibit promising potential in areas such as robotics, sensor technology, and biomedical applications, as they transform their shape and dimensions when exposed to an electric field. The photonic interaction of light with electroactive materials even enables the conversion of light energy into mechanical energy [13]. Another aspect of adaptability is the development of electronically controlled smart windows [14] for use in buildings and automobiles, boasting the ability to adjust their transparency as required. As a whole, smart materials constitute a dynamic and pivotal domain of modern scientific and technological exploration, offering a broad spectrum of applications across various industries [15].

Laser processing, recognized for its high precision, has become indispensable in various areas of industry [16]. Laser technology is widely employed for cutting metallic and non-metallic materials with exceptional precision, finding applications in diverse sectors, from automobile manufacturing to the aerospace sector [17,18]. For instance, laser cutting plays a pivotal role in shaping shape memory alloys, allowing for the production of intricate miniaturized devices used across a spectrum of applications [19–21]. At the same time, laser technologies facilitate the production of high-quality engravings and markings on various materials, serving industries like jewelry, electronics manufacturing, and the production of medical devices [22,23]. Laser welding, on the other hand, allows for the creation of strong joints without the need for additional materials, making it a valuable process in the production of aviation and aerospace systems [24–26]. The application of lasers in interaction with smart materials opens the door to more innovative and adaptable technologies, such as the development of intelligent products capable of modifying their properties through laser manipulation [27–29]. These fields are continuously advancing, and forthcoming progress in these areas could result in a broad spectrum of practical applications.

Enhancing the intelligence of materials using laser processing stands as a modern approach, offering the development of adaptive materials. Laser processing makes it possible to modify the structure and properties of materials, thus endowing them with "smart" attributes. This versatile technique allows to modify the surface [30], to synthesize and process of atomically thin two-dimensional materials [31]. Moreover, laser processing permits the creation of micro- and nanostructures on material surfaces, enabling the modification of properties such as adhesion, hydrophobicity, and others. Notably, it facilitates the creation of self-cleaning surfaces [32–34]. Laser remelting of the near-surface layer emerges as an effective method for microstructure manipulation, leading to reductions in thermal conductivity and resistivity. These changes translate into enhanced thermoelectric performance in metallic materials, as demonstrated through the case of the full-Heusler compound Fe_2VAl in [35].

Laser irradiation can induce a photothermal reaction in materials, which results in changes in their mechanical properties. Laser processing can be used to change the shape and dimensions of a material by heating and cooling it. This is beneficial for creating shape memory materials that are activated using laser beam heating [36,37]. Laser processing can be used to activate or introduce functional additives into a material, enhancing its properties [38,39]. For example, laser-doped selective emitter diffusion techniques have become mainstream in solar cell manufacture [40]. This method is also a promising one-step method for creating conductive micropatterns for electronic devices and sensors [41].

Laser microfabrication can be employed to create micro-electro-mechanical systems (MEMS) with adaptive properties, such as microactuators and microsensors [42–44]. Laser processing can also be used to create optical structures and waveguides on the surface of materials, which can be useful for developing smart optical devices for photonics and optoelectronics [45–47]. All of the above-mentioned methods can be adapted for various materials, including metals, polymers, glasses, and composites. They have applications in diverse fields such as medicine, electronics, aerospace, and the development of smart technologies and sensors [48]. These are just a few examples of possible ways to create smart materials using laser processing, and research in this area continues to advance.

It is worth noting that achieving precision in laser processing and controlling power density distribution for material modification are of paramount importance. Current optical systems have their limitations, which can only be circumvented by adopting an inefficient approach of selecting materials with broader temperature tolerance when designing laser modification processes. A more contemporary solution involves the utilization of computer-synthesized diffractive optical elements (DOEs) for shaping laser beams, enhancing the precision of power density distribution [49].

The primary goal of this article is to analyze structured data in the field of developing smart materials using laser technologies. During the analysis, special attention is given to evaluating the potential and effectiveness of laser processing for addressing various tasks and challenges. Methods for modifying materials by laser irradiation, including changes to their structure, properties, and shape, are examined. Prospects for creating smart materials with use of laser irradiation and their potential applications are discussed. This research is considered promising and holds significant practical value. It is expected that progress in the creation of smart materials using laser processing will have a substantial impact on various industrial sectors.

2. Laser Modification for Smart Materials

Laser modification is a powerful technique employed to modify the physical and chemical properties of materials, offering a wide array of applications and the ability to create smart and intelligent materials [50]. By utilizing a laser beam, the material's surface can be heated or melted, enabling precise changes in its structure and properties [51,52]. This can involve the creation of micro- and nanostructures on the material's surface, influencing its mechanical, optical, or electronic characteristics [53]. One of the notable features of laser material modification is the precise control of laser parameters, such as power, pulse duration, and frequency, allowing for fine-tuned material changes. As a result of laser modification, a material's properties can be tailored to specific tasks. This may include enhancing mechanical strength, improving adhesion to other materials, modifying optical characteristics, and even achieving superhydrophobic and self-cleaning surface properties [54–56].

To create smart materials, laser modification can be carried out in several ways. Laser shock treatment is used to form gradient nanostructures in the surface layer, which is one of the methods of surface intensive plastic deformation under extreme conditions [57,58]. Laser hardening selectively heats the material's surface to enhance its hardness and wear resistance, resulting in smart materials with improved durability and resistance to wear and tear [59–61]. Typically, this process enables the transformation of only the near-surface layer, but in the case of thin elements, it is feasible to harden the entire depth of the material [62]. To optimize the laser hardening process of a thin-walled medium manganese steel sample using oscillating beam technology, a simulation was conducted. The simulation involved defining the power distribution and virtually determining the oscillation frequency. This approach successfully led to the modification of the shape of the hardened zone during the experimental laser hardening process using a disc solid-state laser beam source, applying a power level of 1200 W (Figure 1).

The laser hardening process for medium and high-carbon steels entails locally raising the temperature and then self-quenching at rapid cooling due to the high thermal conductivity of the metal, leading to the formation of a martensitic microstructure with greater hardness compared to the original ferrite–perlite microstructure. In [63], laser surface hardening of AISI 420 steel was carried out using a diode laser with a wavelength of 1064 nm. The processing that was aimed at the formation of a hardened surface with slight melting was performed at 480 W power and scanning speed of 20 mm/s; the size of the laser spot with a top-hat profile was 3 mm. In Figure 2, the microstructure of the cross-section of the laser-hardened AISI 420 steel, examined using a stereo microscope, is displayed. The melt pool had a depth of approximately 370 μm, and each track measured about 2100 μm in width, with slight overlapping. The geometry of the melt pool is related to the process of heat input, which is influenced by laser power and scanning speed. The modification of these parameters affect the hardening depth. Thus, increasing the laser power or decreasing the scanning speed leads to an increase in the hardening depth.

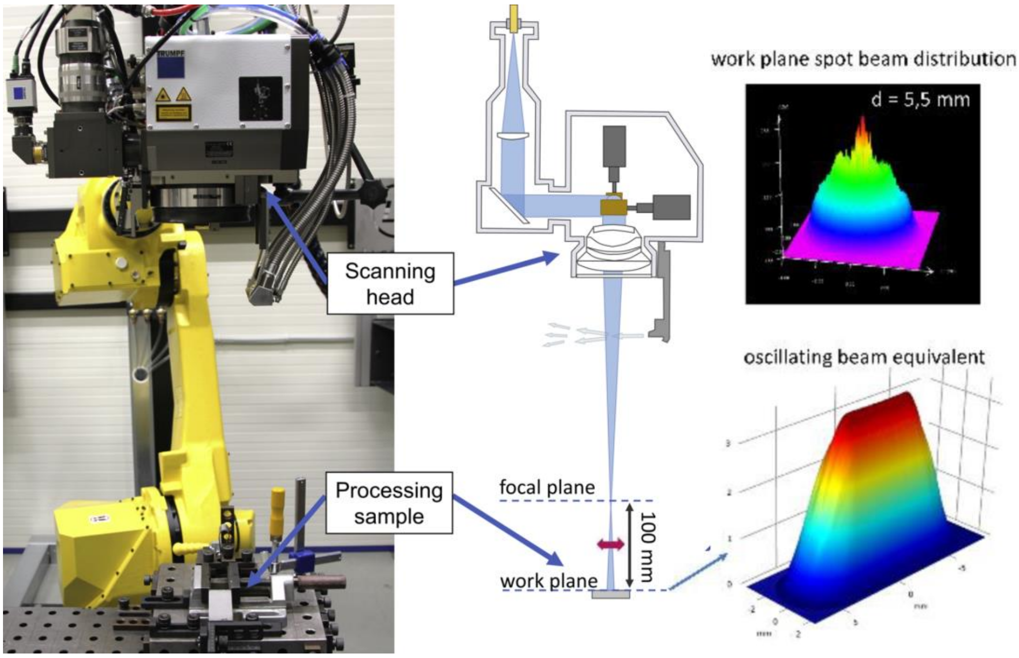

Figure 1. Schematic of the laser hardening process illustrating the beam power distribution in specific planes for experimental studies [62].

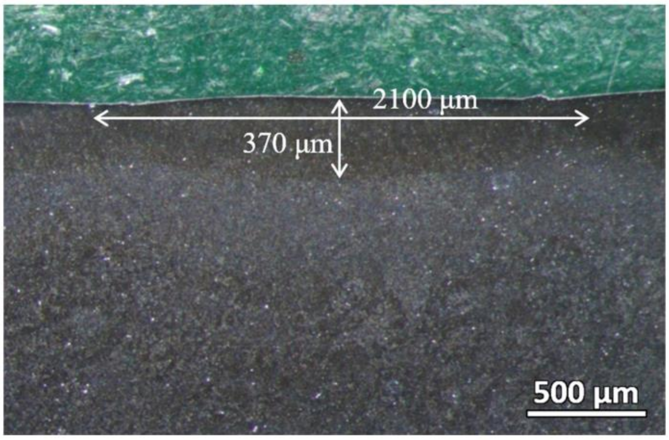

Figure 2. The microstructure of the cross-section of the laser-hardened AISI 420 steel [63].

Laser alloying involves melting a thin near-surface layer of the material and introducing alloying elements or compounds, imparting unique properties such as enhanced corrosion resistance and electrical conductivity [64–66]. Laser boriding of martensitic aging steels has proven to be highly effective in increasing wear resistance. The study in [67] demonstrates that changing laser irradiation parameters, such as laser beam energy and scanning speed, influences the boriding process results in a variety of microstructures in the obtained boronized layers. These microstructures range from hypoeutectic with a low boride content to mixed borides, aligning with the Fe-B phase diagram (Figure 3). The surface laser alloying process involved a fiber laser machine with a wavelength of 1070 nm. Significant processing parameters included a laser power of 300 W, a laser spot diameter of 1 mm, and a variable laser operating speed ranging between 500 and 1500 mm/min. This laser boriding method significantly improves wear resistance in martensitic aging steels, enhancing it by up to 7.5 fold.

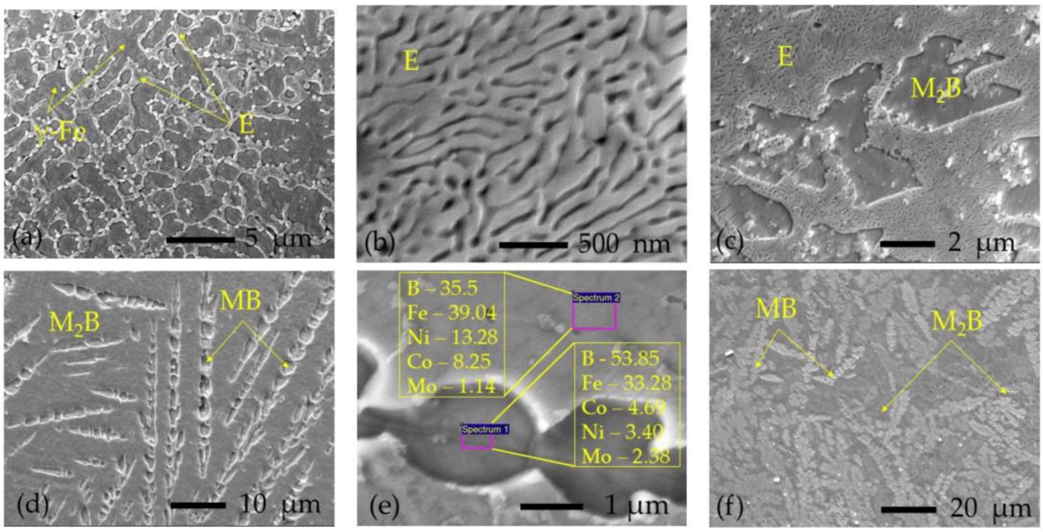

Figure 3. SEM micrographs of laser-boronized layers with different microstructures: (**a**) hypoeutectic microstructure with primary dendrites of γ-Fe solid solution (γ-Fe) and boride-based eutectic (E); (**b**) a fully eutectic microstructure; (**c**) a hypereutectic microstructure with (Fe, Ni, Co)$_2$B (referred to as M_2B) borides surrounded by eutectic (E); (**d**) dendritic higher (Fe, Co, Ni, Mo)B (referred to as MB) borides in a matrix of lower M2B borides; (**e**) an enlarged view of the microstructure shown in (**d**) with marked points for X-ray microanalysis and its results in atomic percentage; (**f**) an example of a microstructure with a mixture of borides exhibiting the highest achieved hardness [67].

Laser doping introduces specific elements or dopants into the material's surface layer, modifying its electronic properties and enhancing semiconductor characteristics [68]. In such cases, subsequent laser annealing can achieve high crystallinity comparable to conventional thermal furnace annealing, but with significantly lower heat input or thermal budget [69]. Laser modification can also activate functional groups on the material's surface [70,71], allowing the creation of smart materials with functional properties, such as chemical sensing for the destruction or inhibition of microorganisms [72].

Laser surface modification can be used to create biocompatible materials for medical implants, with controlled surface properties that promote tissue integration [73–75]. Laser-modified surfaces can improve the adhesion of electronic components or create specialized surfaces for MEMS and sensors [76]. The study in [77] introduced a novel technology for precision manufacturing of quartz resonators for MEMS. This approach relies on laser-induced chemical etching of quartz. The key processing steps involve femtosecond UV laser treatment of alpha quartz plates with Z-cuts, coated with Cr-Au, followed by wet etching. The laser chemical etching process utilized a laser system with pulse widths ranging from 270 fs to 10 ps. It generated pulses with a wavelength of 343 nm, reaching a maximum energy of 40 μJ at a frequency of 175 kHz. The laser output was scanned using low group delay dispersive mirrors and a Newson galvanometer scanner with an F-Theta lens. A visual comparison of etched quartz surfaces with and without prior irradiation is presented in Figure 4. This fabrication method, employing femtosecond laser-induced chemical etching, enables the attainment of superior surface quality using the same wet etching parameters.

Laser-induced surface structures have diverse applications, also in antireflective coatings and high-transparency glasses. For the creation of antireflective coatings, femtosecond laser pulses, with a central wavelength of 1045 nm, a pulse width of 700 fs, and a frequency of 100 kHz were utilized [78]. In the production of high-transparency glasses, a Yb:KGW laser amplifier was employed to generate a linearly polarized femtosecond laser with a central wavelength of 1030 nm, a frequency of 10 kHz, and a pulse duration of 216 fs. The laser beam was focused by a convex lens [79]. Smart materials with laser-modified surfaces can be used in automotive components to improve the wear resistance and reduce the friction [80–82]. The results of various processes, such as laser remelting, laser texturing, and laser shock hardening, demonstrated that fluence was the most critical factor influencing the surface roughness and the microstructure. The optimization of laser parameters can minimize such defects and modulate specific morphology. Furthermore, oxide films produced through femtosecond laser deposition have the potential to manage radiative thermal properties and serve as active energy-saving windows for buildings, satellites, and spacecraft [83]. The described process, outlined in [83], utilized a laser fluence of 0.27 J/cm^2 for ablating the vanadium oxide target, employing a solid-state Ti:sapphire laser/amplifier. Thus, laser surface modification stands as a versatile technique for crafting smart materials by tailoring the surface properties of diverse materials. Its precision in controlling surface features enables the development of materials with adaptive characteristics suitable for a wide range of applications.

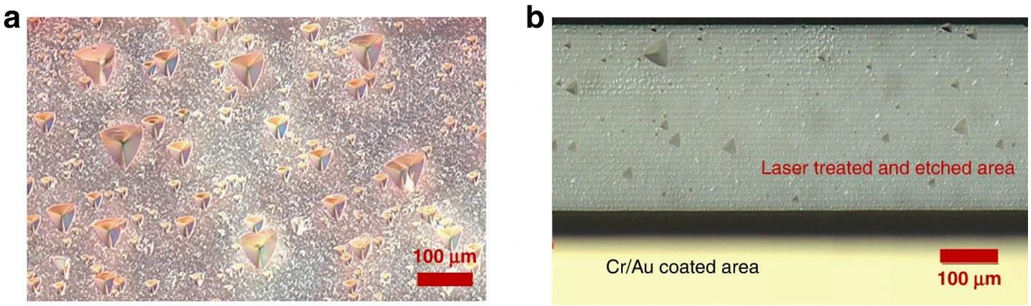

Figure 4. Differential interference contrast (DIC) microscopy images of wet-etched quartz surfaces, with an etch depth of 100 µm: (**a**) quartz surface after 4 h of etching without laser treatment before etching; (**b**) quartz surface after 4 h of wet etching under the same conditions as in (**a**) but after laser treatment before etching [77].

The fabrication of smart materials using laser surface modification offers a range of advantages. It enables precise and selective change in a material's surface properties while preserving its bulk properties. This method provides high precision for targeted adjustments to specific areas on the material's surface. The laser modification method is highly customizable, allowing for the creation of materials with tailored surface properties to meet specific application requirements [84–86]. This method can be closely monitored and controlled to ensure consistent and high-quality surface modifications. It can be applied to a wide range of materials, including metals and alloys, polymers, ceramics, and composites [87–89]. These features make laser surface modification an effective technique for creating smart materials with customized surface properties that can intelligently respond to various impacting factors, offering diverse applications in engineering, electronics, medicine and biotechnology, as well as in other fields.

Thus, laser material modification is a highly customizable and precise process that allows for the individual tailoring of material surface properties. This technology finds applications in various fields, including medicine, electronics, engineering, and biotechnology. Creating smart materials using laser modification opens up new horizons for developing innovative products and devices with intelligent and adaptive surface properties, making this method a crucial tool for future technological advancements and addressing current challenges.

3. Harnessing Photothermal Reactions and Functional Additive Introduction

Laser modification allows one to utilize the possibilities of photothermal reactions and encompasses the introduction of functional additives to transform material properties. The creation of smart materials through photothermal reaction energy allows for the controlled modification of material properties by using laser beams to manipulate their physical characteristics. Photothermal reactions involve the utilization of laser beams to heat materials, ultimately inducing changes in their structure and properties [41,90]. The process begins by selecting a material capable of absorbing laser radiation, typically within a specific wavelength range [91]. The laser beam is precisely directed to the material's surface, where its energy is efficiently converted into thermal energy. The temperature increase achieved can be localized and extremely precise due to the focusing of the laser beam [92,93]. Under the influence of laser irradiation, a photothermal reaction takes place, resulting in modifications to the material's internal structure and properties. These changes may encompass alterations to the crystalline structure, molecular orientation, or other physical parameters of the material. To achieve the desired material changes, it is crucial to control laser processing parameters, including laser beam power, duration of exposure, and the precise location of irradiation [94]. As a consequence of the photothermal reaction, the material can acquire "smart" properties, leading to changes in its optical, mechanical, or electrical characteristics, depending on the level or duration of laser exposure [95]. This capability enables the creation of materials with adaptive properties. Photothermal reactions play an important role in the production of materials that respond to specific therapeutic or diagnostic laser procedures [96,97]. By initiating a photothermal reaction through laser irradiation, precise control and modification of material properties are achieved, making them "smart" and adaptable for a wide range of applications.

The development of smart materials can also encompass the integration of specialized additives or compounds through laser processing. These functional additives have the capacity to introduce novel properties and functionalities to materials [98,99]. For instance, in [100], a study aimed to enhance the bioactivity and wear resistance of titanium and its alloys for potential implant applications. This was achieved through laser cladding, resulting in a multilayer Ca/P (calcium/phosphorus) bio-ceramic coating on the surface of Ti6Al4V alloy using hydroxyapatite and Ti powder as cladding precursors. The laser cladding system featured a medium-power fiber laser and a laser head connected through a QBH standard connector for efficient interchangeability. Laser cladding parameters included a 400 W laser power, 3 mm/s scanning speed, 2 mm spot diameter, and a 30% overlap rate. Figure 5 illustrates the laser cladding process employed to produce the multilayer Ca/P bio-ceramic coating. The resulting coating displayed good biocompatibility (Figure 4), similar to the commonly used Ti6Al4V alloy for medical implants and showed in vitro bioactivity by facilitating hydroxyapatite deposition through ion exchange in an SBF solution, unlike the titanium alloy substrate. Additionally, the coating demonstrated enhanced wear resistance compared to the Ti alloy substrate.

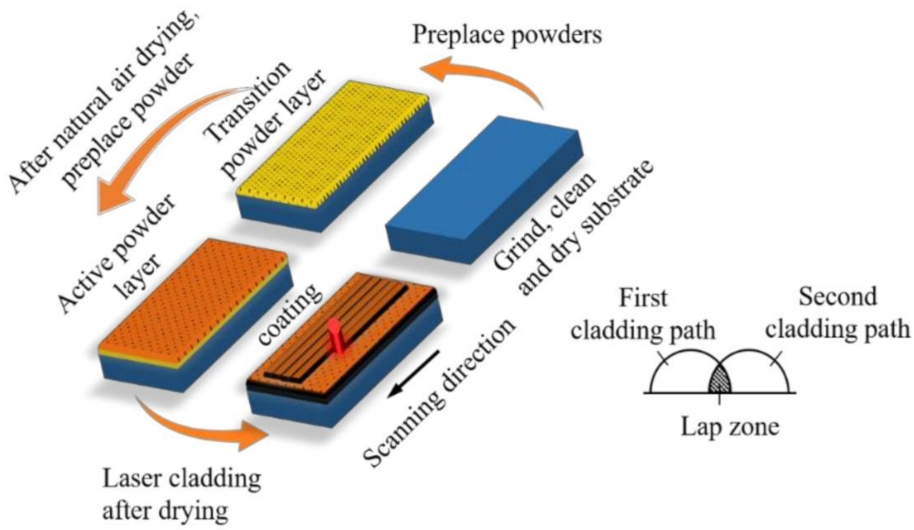

Figure 5. Laser cladding process employed to produce the multilayer Ca/P bio-ceramic coating [100].

Using laser processing, various methods are available for the introduction of functional additives into materials. Alloying, for instance, involves introducing elements or alloys to enhance a wide range of material properties, such as strength, hardness, and corrosion resistance. Cladding, on the other hand, revolves around the application of a layer of one material onto the surface of another, thereby modifying its characteristics [52,101,102]. It is worth noting that the improper selection of cladding process parameters and the mismatch of thermophysical properties between the cladded layer and the substrate material can lead to the development of substantial residual stresses during rapid cooling and heating phases, potentially resulting in various types of cracks [103]. In [104], NiCrSiBC-WC composite coatings were studied with different WC mass ratios on carbon steel substrates, revealing that 40 wt.% WC coatings were crack-free, while those with 50% and 60% WC displayed cracks (Figure 6a). The integrated control system used at the workstation was finely tuned with specific processing parameters: a laser power of 1 kW, a laser spot diameter of 2.5 mm, a laser scanning speed set at 1200 mm/min, and an overlapping rate fixed at 40%. Figure 6b displays metallographic microscopy images of cladding coatings with different WC types in Ni60 coatings: spherical, shaped, and flocculent [105]. The processing was conducted using a semiconductor laser and a five-axis numerical control system. Composite powders were conveyed using coaxial-powder feeding technology. The processing parameters for the cladding layer were specified as follows: a laser power of 1.5 kW, a laser scanning speed of 240 mm/min, a powder feeding rate of 7 r/min, a spot size measuring 4×5 mm, with an overlapping rate set at 40%. It was determined that under the same laser cladding process conditions, the addition of different WC particles has a different effect on the performance of Ni60-30 wt.% WC coatings.

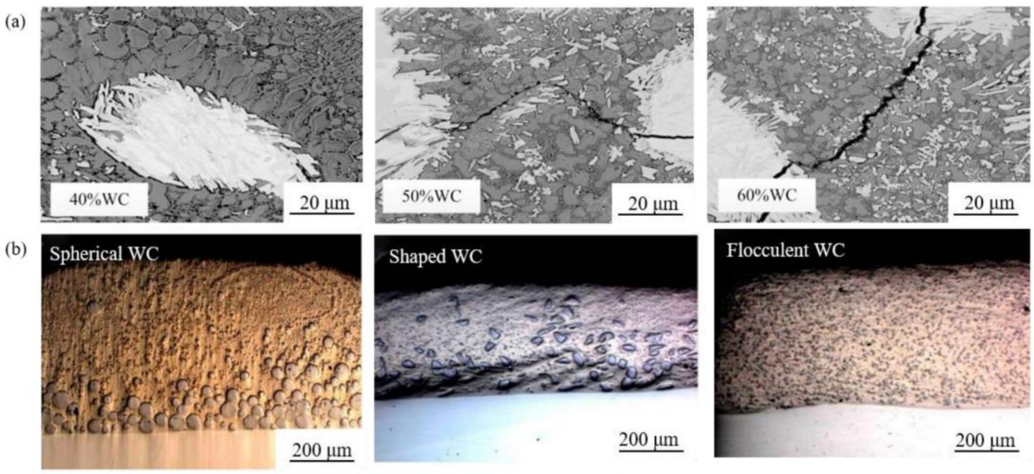

Figure 6. Influence of cladding materials on the microscopic morphology of the coating. (**a**) Microstructure of NiCrBSi-WC coatings with variable WC contents [104]; (**b**) microscopic images of different WC-based coatings in Ni60-30 wt.% WC composite coatings [105].

To produce top-quality laser cladding coatings, the interplay between processing parameters, microstructure, and mechanical properties is thoroughly examined in [106]. In addition, the study in [107] proposed optimizing the laser cladding process parameters through intelligent system optimization algorithms. Cladding can also be achieved through the use of transition layers [108], and the process itself can lead to the creation of functionally graded materials [109] and refractory high-entropy alloys with distinct microstructures and properties [110,111]. The application of laser cladding for the fabrication of high-entropy alloys is thoughtfully presented in [112,113]. This approach, which introduces functional additives into materials using laser processing, contributes to the creation of smart materials with tailored and enhanced properties, promising a wide array of applications.

Doping, on the other hand, involves the introduction of specific elements, known as dopants, into the crystalline structure of a material. This process is carried out to modify the material's electronic properties, encompassing conductivity and optical characteristics [114]. Laser processing comes into play when introducing nanoparticles or creating nanostructures to enhance a material's conductivity, optical attributes, or other relevant characteristics. Moreover, introducing functional additives onto a material's surface using laser processing can lead to changes in its adhesion, wettability, or chemical reactivity. Integrating functional elements like quantum dots or fluorophores using laser processing can result in the development of sensors and detectors with tailored functionality [115]. This approach allows for the creation of materials with unique functional characteristics, making them customizable for various applications. Notably, in [116], the laser doping method was employed, with the application of an ultraviolet nanosecond laser, to co-dope with fluorine and induce an N-type transition in phosphorus-doped germanium. Similarly, in [117], laser doping was used for nitrogen doping in 4H-silicon carbide. A KrF excimer laser with a wavelength of 248 nm was utilized in the experimental study. The pulse duration was 82 ns, while the repetition frequency was set to 100 Hz. Employing a slit, the laser beam was narrowed near the center, creating an area of 300 $\times$ 300 µm on the sample surface. During the experiment, the laser irradiation frequency ranged from 1 to 200 shots per location by adjusting the sample scanning speed. The laser irradiation fluence was set within the range of 2.2 to 3.4 J cm^{-2}. In [118], this method was applied for heavy doping of thin silicon-on-insulator layers in conjunction with laser thermal annealing. These examples underscore the versatility of laser doping as a mean for modifying electronic properties in different materials for specific applications.

It is worth noting that annealing plays a pivotal role in the semiconductor industry, serving as a critical process for optimizing semiconductor material properties. Annealing involves controlled heating and cooling to enhance the crystalline structure, minimize defects, and manage electrical characteristics. To meet the growing demand for low total heat input methods, especially driven by innovations like 3D integrated circuits, pulsed laser annealing has emerged as a promising technique. Pulsed laser annealing offers high dopant activation levels and minimal surface roughness, making it well-suited for various semiconductor applications [119]. Numerous studies delve into the applications of laser annealing. In [120], the paper discussed the preparation and characterization of ZnO nanofilms (ZNFs) on silicon substrates using a sol-gel-assisted spin-coating process. These ZNFs were modified by Nd:YAG pulsed laser annealing at specific wavelengths, resulting in improved structure and electrical properties. The samples were exposed to Nd:YAG laser beams at varying wavelengths, specifically 1064 nm, 532 nm, and 355 nm. Each wavelength received 5 pulses, with an energy fluence of approximately 650 mJ/cm^2, a frequency of 1 Hz, laser energy set at 500 mJ, and a window area of about 0.8 cm^2. In [121], a comprehensive analysis of the green laser annealing method for phosphorus-doped silicon was presented.

Additionally, the study in [122] highlighted the successful solid-phase recrystallization of partially amorphized silicon-on-insulator structures using pulsed ultraviolet nanosecond laser annealing. This approach achieved high dopant activation rates with a low overall heat input, positioning it as a promising technique for 3D sequential integration. In Figure 7, TEM images showcase a cross-section of a 22 nm-thick silicon-on-insulator structure with phosphorus implantation, revealing the impact of sub-melt multi-pulse ultraviolet nanosecond laser annealing (UV-NLA). The samples were processed with UV-NLA using a device equipped with a XeCl excimer laser with a wavelength of 308 nm. The laser had a pulse duration of 160 ns and operated at a frequency of 4 Hz. Spatial homogenization of the laser beam was performed to achieve consistent results, ensuring a non-uniformity level below 3%, and generating a top-hat beam, measuring 15 $\times$ 15 mm^2. The observations highlight that 30 laser pulses at 0.58 J/cm^2 can induce partial recrystallization in the amorphous Si layer, while 100 pulses at the same energy density result in complete recrystallization. This emphasizes the efficacy of UV-NLA in a sub-melt multi-pulse mode, achieving a progressive solid-phase recrystallization of the amorphous layer from the crystalline seed.

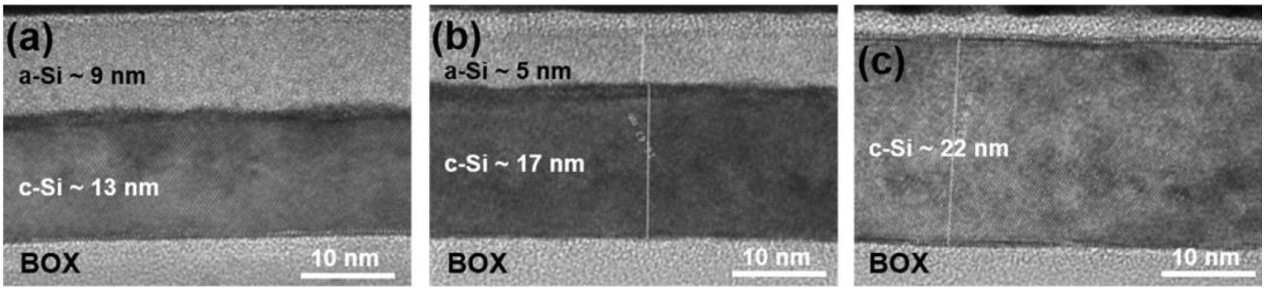

Figure 7. TEM images of cross-sections of 22 nm-thick silicon-on-insulator structures: (**a**) as-phosphorous-implanted and after sub-melt multi-pulse UV-NLA at 0.58 J/cm^2 with (**b**) 30 or (**c**) 100 cumulative pulses [122].

Accordingly, laser modification, using photothermal reactions and the introduction of functional additives, allows for precise control and modification of material properties, making them adaptable for various applications. Photothermal reactions involve localized heating through laser irradiation, leading to structural and property changes in materials. The introduction of functional additives, including polymers, nanoparticles, and metals, enhances materials with new properties and functionalities. These smart materials find applications in electronics, aerospace, medicine, and environmental monitoring.

4. Laser Surface Modification by Direct Laser Interference Patterning (DLIP)

DLIP for surface modification of materials utilizes coherent laser beam interference to create functional periodic microstructures, offering advantages over alternative methods. It stands out for its capacity to directly create large-scale microstructures, varying between centimeters to tens of nanometers, showcasing high speed and versatility. The distinguishing feature of DLIP is that it does not require focused laser beams, which enables high-performance processing with a substantial depth of focus and expanding structuring possibilities through laser parameter variations. This makes DLIP a potent and efficient technique for modifying surface properties across a spectrum of technological applications, encompassing electrical, optical, and tribological domains. The studies [123,124] provided a comprehensive discussion of direct laser interference patterning (DLIP), a high-throughput surface structuring method using overlapping laser beams, with applications in industries like photonics, optoelectronics, nanotechnology, and biomedicine. Figure 8 showcases the DLIP treatment of ~500 nm-thick indium tin oxide (ITO) thin films on glass substrates using a DLIP workstation equipped with a solid-state ultrashort-pulse laser with a maximum output power of 100 W and a pulse frequency of 1 MHz. The laser operated at a wavelength of 1030 $\pm$ 10 nm, with a frequency of 50 kHz, and a pulse duration of 900 $\pm$ 100 fs. SEM images were taken at varying fluence levels to assess the induced microgroove morphology. In Figure 8a, the SEM image displays the untreated ITO surface, while Figure 8b,c depict the DLIP-treated surface at F = 250 mJ cm^{-2}. The DLIP-treated sample exhibits a well-defined periodic array of grooves, and on the valleys of the texture, laser-induced periodic surface structures (LIPSS) are evident. LIPSS features align perpendicular to the laser polarization, extending on both the bottom and sidewalls of the texture. Spatial frequencies of DLIP and LIPSS are identified, with a spatial period of Λ_{DLIP} = 5.0 $\pm$ 0.1 µm for DLIP and Λ_{LIPSS} = 230 $\pm$ 20 nm for LIPSS [124].

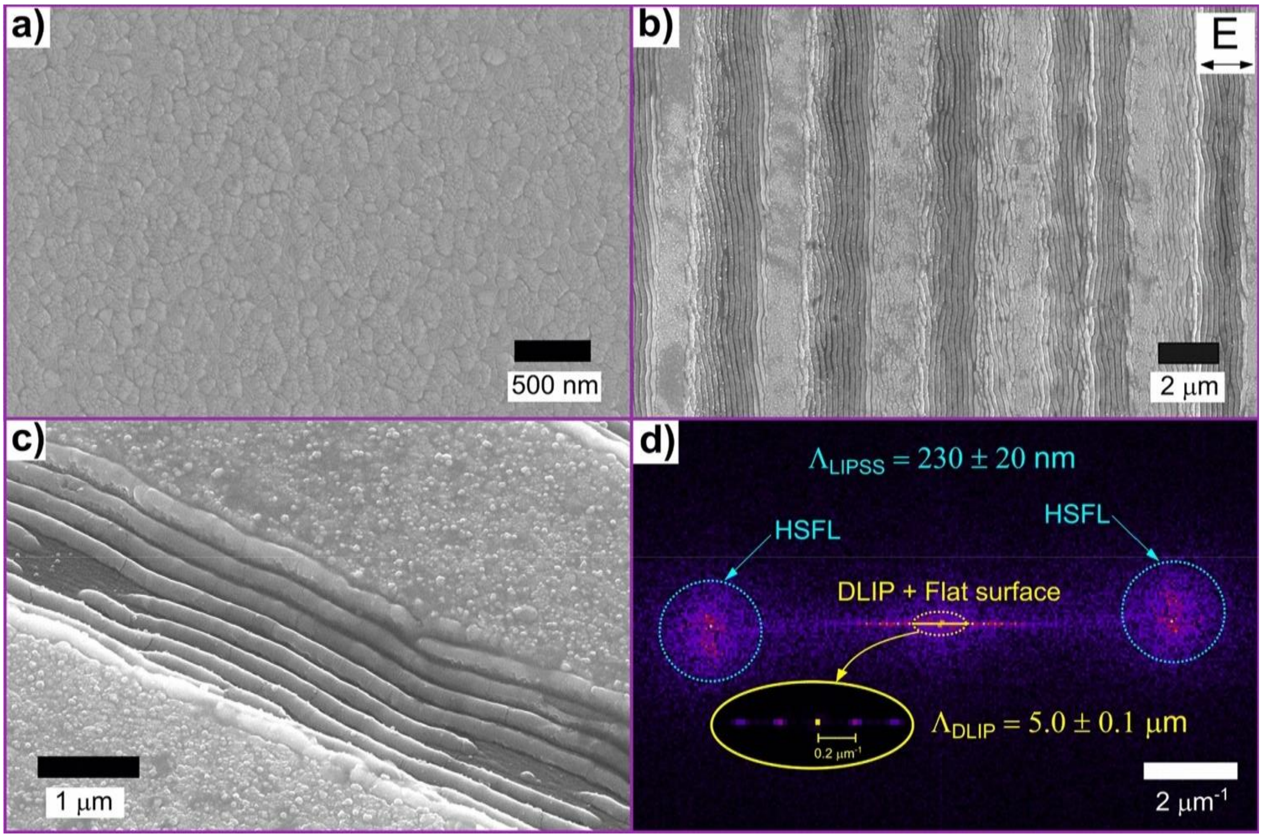

Figure 8. SEM images of (**a**) untreated ITO surface and (**b**) patterned surface at F = 250 mJ cm^{-2}. The electrical field's polarization direction is indicated by the double arrow. (**c**) Tilted view of the ablated area of the sample. (**d**) Absolute value of the two-dimensional Fast Fourier Transform (2D-FFT) applied to (**b**) with a zoomed view of the center frequencies. The double-lobes shapes corresponding to High Spatial Frequency LIPSS are marked by dotted circles [124].

The process of microstructuring in DLIP can engage either photothermal, photochemical, or a combination of these mechanisms, depending on the interaction between laser light and the utilized materials [125]. In [126], the DLIP process scheme was presented (Figure 9). The influence of pulse duration and pulse-to-pulse overlap was investigated. The study provides insights into surface phenomena and demonstrates efficient structuring of challenging, low-absorbing polymeric substrates using ultrashort pulsed lasers (266 fs–15 ps) operating with a frequency of 1 kHz and an emitting IR wavelength of 1030 nm. Here, the surface modification of polyether ether ketones, advanced polymeric materials replacing metals and ceramics, was demonstrated using femtosecond pulses. A laser beam with an elongated shape and a periodic intensity profile, created by the interference of two laser beams, was utilized to remove material from the surface.

In the connector industry, the reduction in friction during the insertion in detachable electrical connections is crucial, commonly achieved through connector design and lubricants. This study utilizes DLIP to create asymmetric saw-tooth structures on Sn-coated Cu plates, showcasing improved performance with lower insertion and higher removal forces, while maintaining electrical behavior [127]. This study utilized a picolaser system, incorporating a laser with a pulse duration of 12 ps and a wavelength of 532 nm. The potential of DLIP has been enhanced by utilizing two beams, enabling the production of surfaces with two-dimensional periodicity and multiple symmetry axes [128]. This technique involved picosecond laser writing of a consistent one-dimensional pattern for different sample orientations, offering versatility in creating diverse two-dimensional periodic structures with varying rotation angles and number of scans. The picosecond laser, operating at a wavelength of 1064 nm and a spectral bandwidth of <0.3 nm, was chosen for its narrow bandwidth, ensuring high-contrast interference patterns throughout the entire spot size.

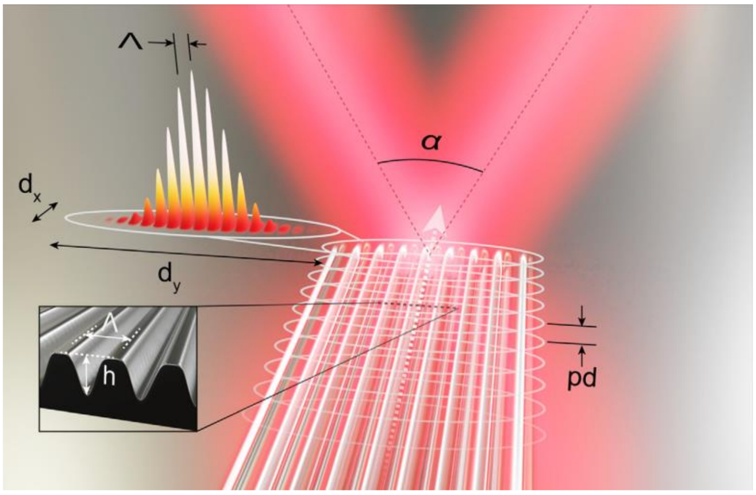

Figure 9. Illustration of the DLIP process. Λ indicates the period of the interference structure formed on the processed material's surface, aligning with the structure's period. The variables h, dx, and dy denote the height of the structure and the dimensions of the elliptically shaped focal spot of the laser beam, respectively, while α represents the angle between the laser beams [126].

In [129], surface structures on 4H-SiC were generated using ultrashort pulsed DLIP (USP-DLIP) and a single Gaussian beam process. Through the utilization of a DOE to split a single beam into two, the interfered beams produced hierarchical structures, encompassing high spatial frequency LIPSS (HSFL) and low spatial frequency LIPSS (LSFL). The aspect ratio control capability of USP-DLIP was demonstrated through experimental results and Raman analysis, indicating a reduction in crystalline SiC peak intensity following USP-DLIP irradiation. The study employed a femtosecond laser with linear polarization, a wavelength of 1030 nm, a pulse duration of 420 fs, a frequency of 100 kHz, a maximum output power of 2 W, and a beam diameter of 2.4 mm (at $1/e^2$). In [130], a single-step method for creating porous photocatalytic surfaces on titanium substrates was introduced by DLIP with picosecond-range pulses. The study showcased the tunability of composition and morphology in the resulting surfaces, allowing customization for applications like antimicrobial surfaces, implant materials, or water treatment, utilizing a DLIP setup with a DOE and prism for versatile beam manipulation. The laser patterning was executed using a picosecond laser with a pulse width of 12 ps, a wavelength of 532 nm, a frequency of 100 kHz, and a maximum average power of 10 W.

In [131], the focus was on integrating a diffractive fundamental beam-mode shaper element, or DOE, into a DLIP optical setup to create a square-shaped top-hat intensity distribution. The research involved measuring and characterizing interference patterns, identifying the system's sensitivity to optical misalignments, and elaborating an optical system for generating square-shaped interference distributions of energy with a flat-top intensity profile. The goal was to enhance the homogeneity of surface patterns in applications involving functionalized surfaces, emphasizing the application of the DOE. In [132], a diffractive beam-shaping element, or DOE, was integrated into a four-beam DLIP setup, demonstrating advantages over using a standard Gaussian beam configuration, including increased structure height, improved pattern uniformity, and enhanced productivity for specific patterns. The experimental investigations utilized a laser four-beam interference setup, resulting in the formation of dot-like interference patterns. This setup included a nanosecond-pulsed laser system operating at a wavelength of 1053 nm, with a maximum average output power of 4 W, a frequency of 4 kHz, and a pulse duration of 6 ns. Figure 10 illustrates the schematic of the experimental setup, along with the interference intensity patterns for the setup with and without a DOE.

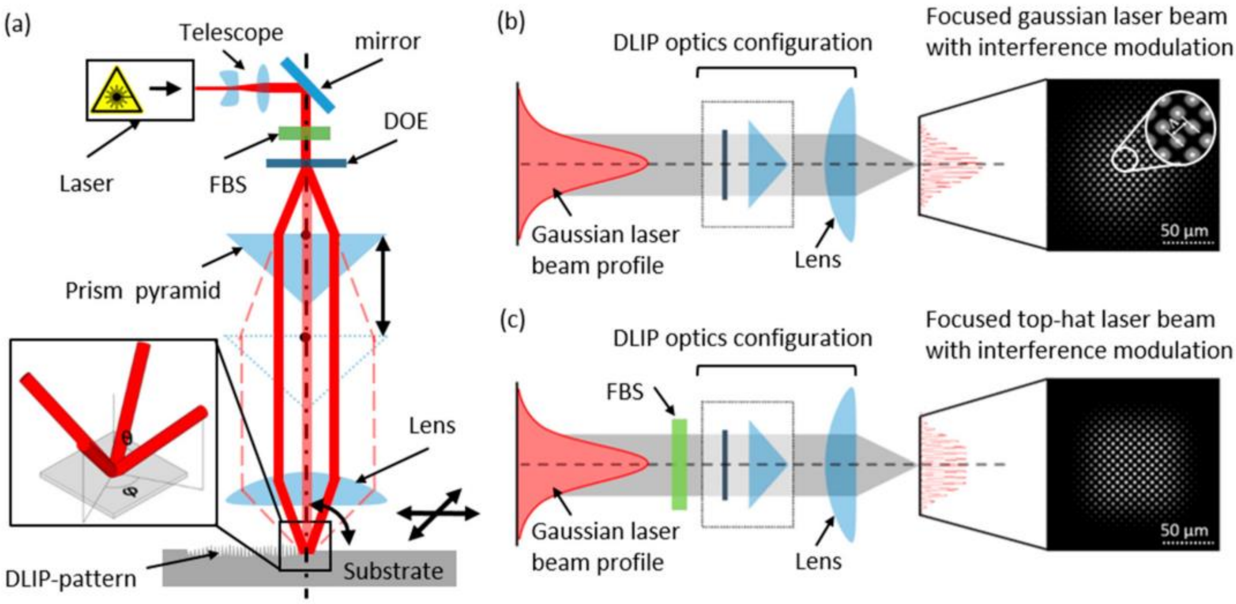

Figure 10. (**a**) Experimental setup features a compact DLIP optical configuration, with the main beam divided into four identical sub-beams using a DOE. Inset displays four symmetrically distributed sub-beams with θ as the incidence angle and ϕ as the azimuthal angle. Interference intensity patterns are illustrated for two setup variants: (**b**) without and (**c**) with a DOE [132].

Designing materials with micro- and nano-scale two- and three-dimensional structures introduces a new opportunity for tailoring material properties and enhancing functionalities. The complexity of such designs requires advanced fabrication techniques, particularly with high resolution on the nanoscale. DLIP emerges as an innovative solution for high-speed patterning of periodic structures. This method involves overlapping multiple laser beams on the material's surface, facilitating rapid and precise customization of material surface microstructures and topographies at industrially relevant scales [133]. Laser-textured surfaces, gaining prominence for their diverse applications and industrial scalability, have been extensively studied in research with the purpose of creating functional surfaces. The study outlined in [134] demonstrates that combining structures with varying feature sizes, produced different techniques like DLIP, direct laser writing, and LIPSS fabrication methods not only enhances specific functions but also imparts multiple functionalities to materials. This includes improvements in surface wetting properties, resistance to ice formation, self-cleaning capabilities, antibacterial performance, and the enhancement of optical properties in polymer materials, designed for manufacturing solar cells and organic light-emitting diodes.

Thus, it has been demonstrated that direct laser interference patterning is a progressive method to fabricate defect-free periodic micro- and nanostructures for a wide range of materials, opening up new possibilities for the formation of functional surfaces. DLIP has been successfully implemented using different pulsed laser sources, processing systems and configurations. Because of the flexibility of DLIP in terms of fabricated geometry, sizes, and its compatibility with a wide range of materials, numerous applications become feasible.

5. Shape Change Manipulation Using Laser Processing

Creating smart materials using laser processing and shape change manipulation is a modern approach that involves using laser irradiation to induce controlled changes in the shape and dimensions of a material. It is particularly useful for developing materials with shape memory properties, making it suitable for 4D processes, such as the creation of objects that can change their shape in response to various cues [135–137]. 4D printing is an emerging technology that extends the concept of 3D printing by adding an additional dimension—time. In 4D printing, the printed object is designed to change its shape or function over time when exposed to specific environmental conditions or external stimuli. The process typically involves printing a structure using materials with special properties, such as shape-memory polymers [138–141] or composites with responsive elements [142–145], ceramics are also finding applications [146–148]. These materials are programmed to react to external factors like heat, moisture, light, or magnetic fields. When the printed object is subjected to the predetermined stimulus, it undergoes a transformation, changing its shape, structure, or properties. The technology holds great promise, as it allows for the creation of objects that can adapt and optimize their performance in real time.

The progress in high-temperature ceramics is hindered due to their extreme melting points and the challenge of crafting complex structures. 4D printing emerges as a solution, enhancing the geometrical flexibility of ceramics. In [146], a ceramic 4D printing method combining laser machining, UV/ozone film deposition, and heat treatment is presented. It induces rapid shape and material changes, allowing versatile structures with tunable bending. Precursors transform into ZrO_2–SiOC ceramics or SiOC glass, showcasing reversible reconfigurability and shape memory.

The 4D printing of metallic materials often employs specific metal alloys with shape memory properties. These alloys can include, but are not limited to the following. Nitinol (Ni-Ti) is a well-known shape memory alloy that consists of nickel and titanium. It is widely used in various applications due to its excellent shape memory and superelasticity properties [149–151]. Copper-based shape memory alloys, like Cu-Al-Mg and Cu-Zn-Al, can be utilized for 4D printing applications, offering good shape memory behavior and mechanical properties [152,153].

Fe-Mn-Si alloys, containing iron, manganese, and silicon, have emerged as a promising option for 4D printing. Recent research highlights their potential, as exemplified by [154], which demonstrated the ability to tailor the microstructure of Fe-Mn-Si shape memory alloys via changes in laser powder bed fusion parameters. Samples were produced using laser powder bed fusion (LPBF) with a 200 W fiber laser machine equipped with a quartz F-Theta lens, resulting in a laser spot diameter of 55 µm. The manufacturing process involved three different scanning velocities: 100 mm/s, 250 mm/s, and 400 mm/s. The laser power was consistently maintained at 175 W for all samples. Additionally, a uniform distance between the centers of the applied tracks was chosen as 100 µm. In [155], the impact of heat treatment and thermomechanical training on both conventional and additively manufactured FeMnSi-based shape memory alloys was studied. Additive manufacturing samples were produced using a LPBF machine equipped with a 1070 nm fiber laser and a spot size of 55 µm. The scanning strategy employed a bidirectional approach without border contour, followed by a 90° rotation between layers. The optimized parameters consisted of a scanning speed of 225 mm/s, a laser power of 175 W, a layer thickness of 0.03 mm, and a hatch spacing of 0.1 mm. Heat-treated, additively manufactured samples exhibited the highest total recovery strain due to smaller grain size and a higher volume fraction of precipitates.

In [156], the study investigated the influence of laser energy density on the properties of Fe-Mn-Si-Cr-Ni shape memory alloys during the fabrication process, thus offering insights for optimizing intelligent structures. Fe-Mn-Si-Cr-Ni samples were produced on a 316 stainless steel substrate using the LPBF machine equipped with a 400 W Ytterbium fiber laser. The hatch spacing and layer thickness were maintained at 0.08 mm and 0.03 mm, respectively. Throughout the fabrication process, volumetric energy densities were adjusted in the range of 42 to 300 J/mm^3 by varying both the laser power (ranging from 100 to 360 W) and the scanning speed (ranging from 500 to 1000 mm/s).

The study in [157] introduces an innovative category of buckling-induced architected Fe-SMAs (BIA Fe-SMAs) composed of Fe-Mn-Si-Cr-Ni, fabricated by 4D printing. These alloys exhibit significant energy dissipation and shape recovery capabilities, thereby enhancing their multifunctionality. The production of samples was conducted using an LPBF machine equipped with a 1070 nm fiber laser featuring a Gaussian intensity distribution, a spot size of 55 µm, and a maximum output power of 200 W. For experimental investigations, the laser power was set to 175 W, the layer thickness to 0.1 mm, and the hatch spacing to 0.03 mm. The applied scanning speed varied between 225 mm/s and 300 mm/s for different groups of samples. In Figure 11, diverse potential practical applications of 4D printed BIA Fe-SMAs are visually explored, showcasing their efficiency in absorbing and dissipating energy in a reusable context.

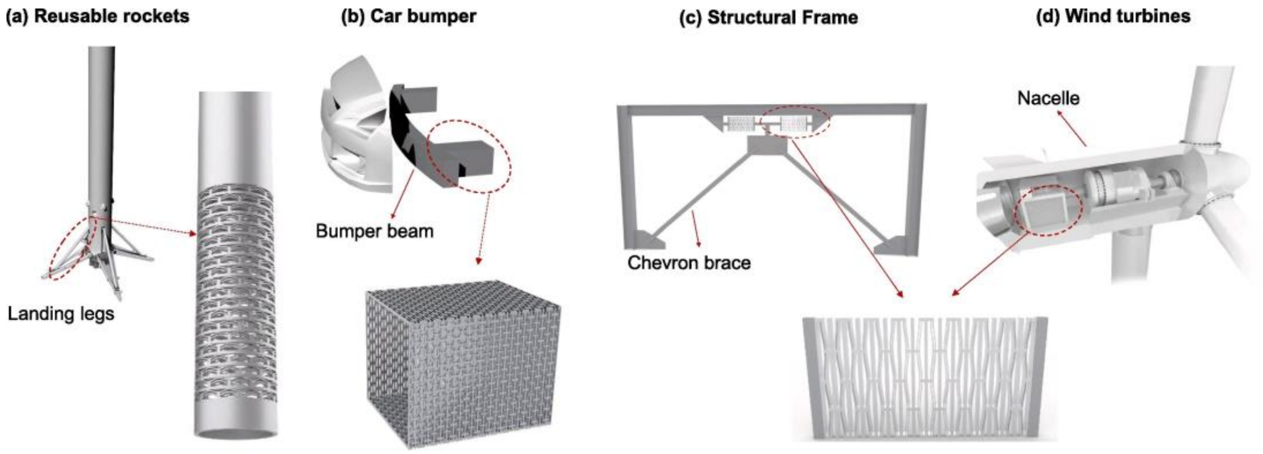

Figure 11. Examples of potential applications for BIA Fe-SMAs in passive impact and vibration isolation. (**a**) Implementation in landing legs for reusable rockets, (**b**) integration into bumper beams, (**c**) vibration isolation for resilient buildings and constructions, and (**d**) passive dampers for wind turbine nacelles [157].

Depending on the desired characteristics, other binary or ternary alloys may be used, such as nickel-titanium-hafnium (Ni-Ti-Hf) [158]. An LPBF machine was configured with an ytterbium fiber laser with a power of 300 W, operating at a wavelength of 1070 nm and featuring a spot size of 80 µm. The input parameters for the fabrication of Ni-Ti-Hf using LPBF encompassed laser power settings of 135 W and 175 W, scanning speeds of 400 mm/s, 600 mm/s, and 950 mm/s, hatch spacings of 135 µm and 140 µm, along with the layer thickness. The advancement of 4D printing has primarily focused on thermal shape memory alloys. Nevertheless, with magnetic shape memory alloys, such as those of the Ni-Mn-Ga system, receiving attention [159]. The choice of alloy depends on the specific application and the desired behavior of the 4D-printed object. Different alloys may offer varying levels of shape memory properties, transformation temperatures, and mechanical characteristics, making it essential to select the most suitable material for the intended purpose.

Applications of shape change manipulation using laser processing can be varied. Shape memory alloys and polymers with laser-induced shape change capabilities are used in minimally invasive medical devices, such as stents and catheters, which can be inserted in a compact form and then expanded to their functional shape within the body [160,161]. Shape memory materials that respond to laser heating are applied in aerospace components, such as aircraft wings and control surfaces, to enable adaptive aerodynamics [162]. Smart materials with shape memory properties are used in robotics to create self-deploying structures and adaptive robotic components [15]. Shape memory alloys can be integrated into consumer electronics, such as smartphones, to enable adaptable form factors or user interfaces [163]. Shape change materials can be employed in automotive applications, such as self-healing or adaptive panels [164,165]. That is, shape change manipulation using laser processing is a versatile technique for creating smart materials with shape memory properties. These materials can be used in a wide range of applications where controlled changes in shape and dimensions are required, offering unique possibilities for innovation in various industries.

Thus, the concept of 4D printing has emerged as an innovative technology that adds a temporal dimension to 3D printing, enabling objects to change shape or function in response to specific environmental stimuli, making it highly adaptable and promising for various applications. The use of polymer, composite, and ceramic shape memory materials, as well as shape memory alloys, such as Nitinol, copper-based alloys, and Fe-Mn-Si alloys, in 4D printing offers a wide range of options, allowing for materials with varying shape memory properties to be chosen based on the specific application requirements. These smart materials are finding applications in the fields of minimally invasive medical devices, aerospace components, robotics, consumer electronics, and automotive innovations, demonstrating their versatility and potential for advancing various industries.

6. Laser-Processed Smart Materials in Photonics and Optoelectronics

The application of laser processing in the development of smart materials for photonics and optoelectronics has opened up new frontiers in advanced technology. This innovative approach involves utilizing laser irradiation to induce controlled changes in the properties of materials, enabling precise modifications tailored to specific optical and optoelectronic requirements [166].

In the field of photonics, smart materials created by using laser processing are applied in the development of reconfigurable photonic devices. As a result of laser-induced heating, materials can undergo controlled and reversible phase transitions, enabling the development of materials with dynamic optical properties that respond to external stimuli such as temperature, light, or magnetic fields. Promising phase-change materials (PCMs) include chalcogenide compounds and transition-metal oxides [167]. Chalcogenide vitreous semiconductors find applications in integrated optics, memory cells, and diffractive-optical elements due to their low absorption in the near and mid-infrared range and reversible phase transitions from amorphous to crystalline states when exposed to short-wavelength radiation. The study in [168] presented an approach for accurately predicting the microstructure and optical response of such phase-change materials during laser-induced heating. This method is crucial for designing programmable photonic devices, particularly for applications like all-optical neural networks and PCM-programmable perceptrons. The samples consisted of 50 nm-thick silicon nitride membrane windows on a 0.5 mm thick silicon substrate, with a 30 nm amorphous $Ge_2Sb_2Te_5$ film deposited using radio frequency magnetron sputtering. The simulation of crystallization and melting processes in amorphous $Ge_2Sb_2Te_5$ involved utilizing a focused Gaussian laser beam. The beam radius ($1/e^2$ intensity) was fixed at 600 nm, while the peak power was adjusted within the range up to 5.0 mW, and pulse durations varied from 10 ns to 1000 ns. These choices of parameters were determined based on the capabilities of the laser testing system. A nanosecond laser was employed for processing. Figure 12 illustrates the results of partial crystallization by changing the laser pulse width from 10 ns to 60 ns at 5.4 mW. In this range, controllable reflectivity is observed, and longer pulses inducing melting and subsequent recrystallization, with forming larger grains in the center and smaller grains around the perimeter. Experimental data align well with simulation results.

In [169], it was demonstrated that subablative ultrashort laser pulses effectively generate well-organized surface nanostructures in chalcogenide glasses. Irradiation utilized ultrashort pulses from the Yb:KGW femtosecond laser system at a 1030 nm wavelength, featuring a pulse duration of 185 fs and a frequency of 200 kHz. The incident laser beam, normally oriented and linearly polarized, was focused through a lens with a 75 mm focal length, resulting in a beam spot diameter on the sample's surface of approximately 70 μm ($1/e^2$). Femtosecond laser exposure was employed to create structured patterns in mid-IR materials, particularly chalcogenide glass ($Ge_{23}Sb_7S_{70}$), with a focus on developing photonic devices, including applications in spectroscopy [170]. Three distinct femtosecond laser systems were employed, each emitting pulses with varying durations. The first system generated 50 and 100 fs pulses at 850 nm using a Yb-doped fiber. The second system produced 150 fs pulses at 1030 nm through a Regen amplifier, while the third system delivered 270 fs pulses, also at 1030 nm, using a Yb-doped femtosecond fiber laser. A 0.4-numerical aperture objective was utilized for the focusing of laser beams on the surface and within the sample volume, resulting in a spot size (defined at $1/e^2$) of 1.94 μm for 1030 nm and 1.6 μm for 850 nm. Figure 13 depicts the applied spatio-temporal beam engineering techniques, utilizing spatial and spectral phase modulation for shaping beams in both spatial and temporal domains.

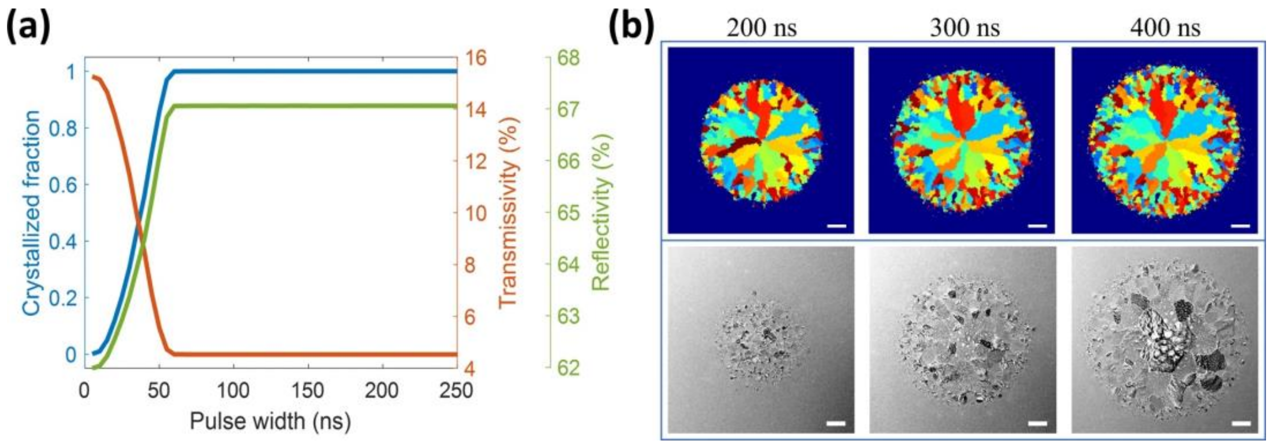

Figure 12. Partial crystallization by changing laser pulse width. (**a**) Crystal fraction, reflectivity, and transmissivity in response to a pulse with different widths: controlled reflectance as a function of pulse duration is observed. (**b**) Crystallographic microstructures resulting from laser irradiation. Upper row: simulation. Lower row: experiments. Scale bar: 200 nm [168].

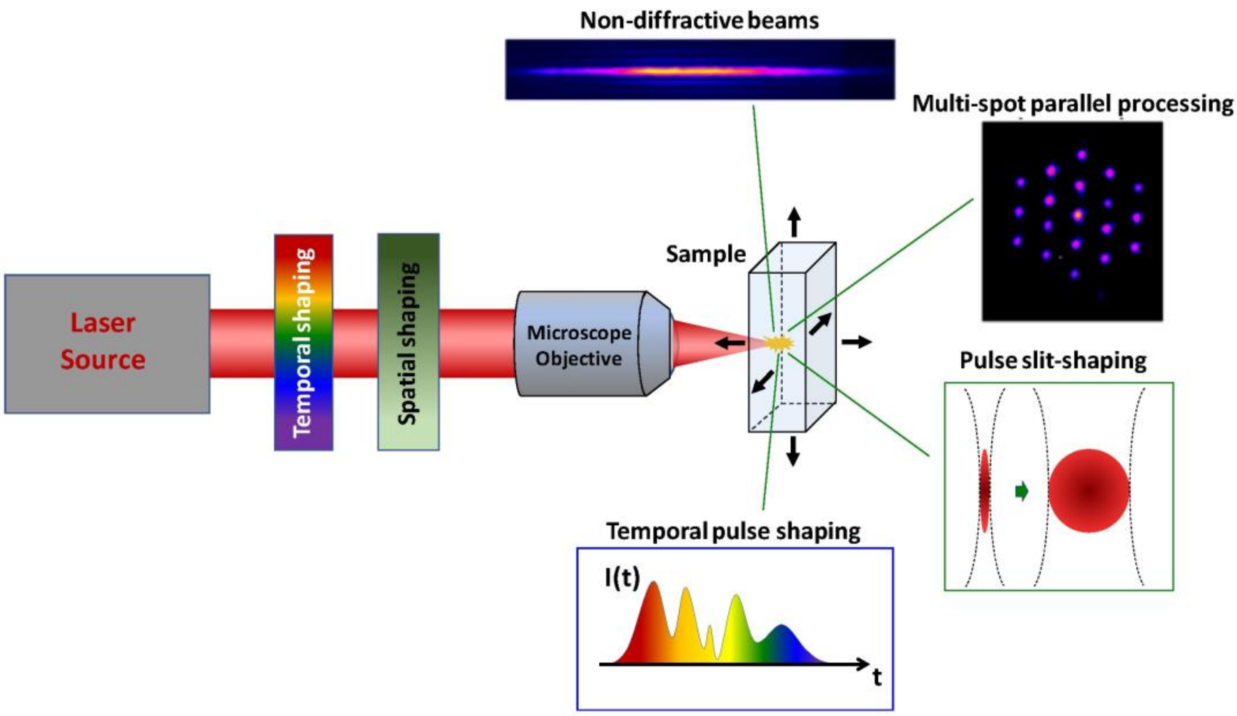

Figure 13. Techniques of spatio-temporal beam engineering employing spatial and spectral phase modulation for beam shaping in space and time domains. Examples encompass the creation of non-diffractive beams, parallel processing, beam slit-shaping, and time-envelope shaping [170].

The study in [171] described the use of ultrafast laser processing to produce multiscale photonic structures in bulk chalcogenide glasses, enhancing their potential for constructing efficient embedded spectrometers and saturable absorbers for integrated photonic applications. A comprehensive structural and optical characterization of germanium antimony selenide (Ge-Sb-Se) films induced by femtosecond laser micromachining was presented in [172], offering valuable insights for the development of versatile photonic devices. Adjusting laser power and scanning speed during laser direct writing allowed the creation of various regions in chalcogenide films. Additionally, the study in [173] investigated the impact of multiple annealing cycles below the glass transition temperature on the response of bulk sulfur-based chalcogenide glasses to ultrafast laser pulses, emphasizing the potential implications of these findings for improving efficient photo-inscription techniques in integrated photonics. Laser-induced phase transitions, capable of adapting the material's refractive index, enabled dynamic control of light propagation. This technology has been employed in creating reconfigurable photonic circuits, optical switches, and modulators, offering enhanced versatility in optical signal processing. These developments will have wide-ranging applications in future intelligent photonic systems [174].

In the field of optoelectronics, laser-processed smart materials play a vital role in the design of responsive devices. Materials engineered to change their optical properties under laser irradiation can be integrated into optoelectronic components, such as light-emitting diodes (LEDs), displays, and sensors. This allows to create adaptive optoelectronic systems that can dynamically adjust their characteristics based on changing environmental conditions. The study in [175] focused on Ge-Sb-Se-Te (GSST) materials, highlighting their remarkable properties as phase-change materials. The research explored both bulk and thin films of these materials, emphasizing their applications in optoelectronic devices, such as switching, metasurfaces, de-multiplexers, and modulation concepts. One of the most common methods for deposition of chalcogenide thin films is the pulsed laser deposition (PLD) technique [176].

Furthermore, laser micromachining, encompassing techniques like laser ablation and laser etching, is instrumental in the fabrication of intricate photonic structures such as diffraction gratings and optical waveguides directly onto materials, allowing for the tailored design of optical components [177,178]. In [178], experimental studies involving bi-layer Si/Ti films were conducted using the circular laser writing system equipped with a continuous-wave DPSS laser, operating with a wavelength of 532 nm and a maximum power of 2 W. The linear scanning speed of the focused laser spot is determined by the radial position of the lens, measuring 0.7 μm during experimental studies. For example, when dealing with a Ti film thickness of approximately 60 nm, the maximum scanning speed during laser writing reached around 200 mm/s. Laser ablation offers precise material removal, enabling the creation of microchannels or cavities with sub-micron accuracy.

Direct laser writing, recognized for its versatility and efficiency in producing intricate photonic devices through localized adjustments in the refractive index of bulk dielectric materials, was widely employed. It accommodated various transparency ranges, including the visible, near, or mid-infrared range [46]. In [179], the femtosecond laser system employed in the investigation had a central wavelength of 800 nm, a frequency of 1 kHz, and a pulse width of approximately 35 fs. A polarized laser beam was generated using a half-wave plate polarizer. An objective lens with a numerical aperture of 0.7 and a magnification of 50× was focused on the core of the TCF. The fiber grating was created by periodically scribing lines along the parallel direction of the core, employing a laser energy setting of 0.3 μJ and a platform with a scanning speed of 20 μm/s. The line length and the period of the fiber grating were determined by the exposure time. In [180], experimental investigations were carried out using laser thermochemical recording on a thin metal film, specifically an ultrathin 10-nm titanium film deposited on a BK7 glass substrate. The experiments utilized a continuous-wave Yb-fiber laser operating at a wavelength of 1070 nm and featuring a Gaussian distribution. The laser source was coupled with an optical module that facilitated the control of scanning speed and allowed for the adjustment of the laser beam diameter to 35 μm at the focal plane. During the track recording, a beam diameter of 85 μm and a scanning speed of 1 mm/s were used. This technology expedites the production of sophisticated optical chips by integrating photonic functions, material ablation, and electrode patterning, simplifying the process by eliminating the need for multiple lithography steps.

Laser annealing plays a pivotal role in modifying the crystal structure of materials, especially semiconductors, to improve their optical and electronic properties, aiding in the development of photovoltaic devices and optoelectronic circuits. Integrating 2D materials into silicon photonic devices holds the promise of significantly enhancing optoelectronic device performance, leading to reduced response times, reduced energy consumption, and a simplified fabrication process. In [181], laser processing emerged as a powerful tool for enhancing 2D material-based photonic devices, unlocking advanced design possibilities for silicon photonic integrated circuits. In [182], laser recrystallization was utilized to produce ultralong single-crystal SnSe wires with a structure conducive to high thermoelectric performance at micro- to nanoscale diameters, presenting potential applications in optoelectronic devices like photodetectors and other components with specific electronic and optical properties.

Laser doping utilizes laser treatment to introduce specific impurities into materials, enabling the customization of their electrical and optical characteristics for various optoelectronic applications [183]. The experimental investigations utilized the second harmonic of a nanosecond-pulsed Nd-laser with a wavelength of 532 nm. Employing two beam splitters in the experimental setup, the energy density was selected within the range of 0.1–0.9 J cm^{-2}. The generation of amplitude-phase thin gratings occurred under the Raman–Nath diffraction conditions, with spatial frequencies set at 90, 100, and 150 mm^{-1}. In contrast, laser-induced functionalization selectively integrates functional groups or nanoparticles onto a material's surface, enhancing its optical and electronic characteristics, providing responsiveness to specific wavelengths or stimuli [184]. These laser-based techniques provide versatile means to tailor materials to meet precise application demands in the areas of photonics and optoelectronics.

Smart materials fabricated using laser technologies have shown great promise in creating highly sensitive optical sensors for a range of applications, including environmental monitoring and medical diagnostics. The study presented in [185] demonstrated advancements in optical fiber sensors through laser micro/nano processing, with a particular focus on fiber Bragg gratings and cladding waveguide structures, as well as explored their practical applications. It also investigated the potential of enhanced Rayleigh backscattering fibers achieved through femtosecond laser dot inscription, revealing innovative sensing capabilities.

In [186], the study explored self-powered wearable optoelectronic devices for mobile visual communication and addressed thermal limitations in flexible inorganic optoelectronics through innovative light-material interface (LMI) technologies, such as nanowelding and laser lift-off, as well as physical interlocking and interfacial chemistry. These developments supported the creation of LMI-based self-powered optoelectronic components like nanogenerators, energy harvesters, and micro-LEDs. Laser micromachining and doping played a crucial role in producing photonic integrated circuits (PICs), integrating various photonic elements on a single chip, thereby improving data processing speed and efficiency [187].

Laser processing plays a vital role in manufacturing high-efficiency solar cells by optimizing semiconductor materials' light-absorbing properties. Using laser technology, have been created micro- and nanostructures on solar cell surfaces, reducing light reflection and increasing sunlight absorption, significantly enhancing energy conversion efficiency [188]. Furthermore, laser-processed materials, including quantum dots, are instrumental in developing next-generation displays with improved color and efficiency. In [189], the study explored advances in DLIP to synthesize semiconductor quantum dots from the II-VI group, particularly emphasizing the solid-state approach using laser-assisted conversion. DLIP was proposed as a potential technique for pixel patterning in quantum dot light-emitting diodes (QD-LEDs) for display manufacturing, offering a simplified, chemical-free solution. Laser-written waveguides and gratings have been integral to optical communication systems, enabling efficient light transmission and routing [190].

Laser processing is harnessed to fabricate specialized optical fibers tailored for telecommunications, medical imaging, and sensing. In [191], the paper detailed the production of GaSb/Si core fibers and a laser restructuring technique that effectively aggregated substantial GaSb regions without inhibiting photoluminescence at room temperature. Figure 14 illustrates the laser treatment of composite fibers. In Figure 14a, thermal emission images depict the initial heating of the fiber, where solid silicon appears brighter than the liquid GaSb/Si alloy due to higher emissivity. Figure 14b shows X-ray computed tomography of the fiber after heating and translation, indicating the accumulation of GaSb. The blue arrow indicates the laser scan direction, and the yellow dashed bar represents the size of the melt zone before laser power reduction, with the liquid composition during the scan being approximately 40 vol.% GaSb. In Figure 14c, EDX elemental maps display the uniformity of silicon and GaSb phase-segregated regions after translation. Red arrows indicate locations where cross-sections were prepared. Figure 14d presents θ–2θ X-ray diffraction data, revealing the appearance of {111} GaSb reflections in the segregated fiber [185].

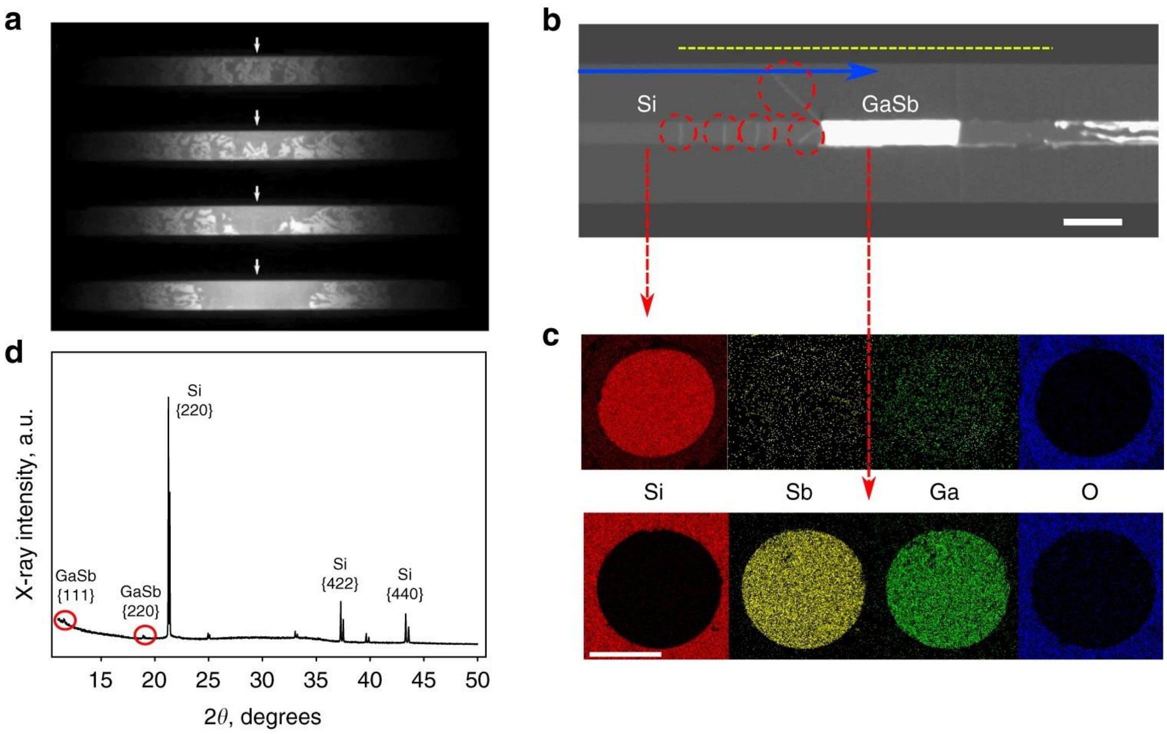

Figure 14. Laser treatment of composite fibers: (**a**) Thermal emission images during initial heating, where solid Si is brighter than the liquid GaSb/Si alloy; (**b**) XCT of the fiber after heating and translation, showing GaSb accumulation (scale bar 350 µm); (**c**) EDX elemental maps of silicon and GaSb regions after translation, with red arrows indicating cross-section locations; (**d**) θ–2θ X-ray diffraction data of the segregated fiber [191].

The study in [192] introduced a laser annealing process for crafting specialty optical fibers with a semiconductor silicon core encased in a glass shell. Figure 15 showcases the investigation of a silicon core fiber (SCF) using a CMOS camera positioned perpendicular to the laser beam. In Figure 15a,b, micrographs depict the SCF being heated by a CO_2 laser beam at different power levels. Real-time monitoring of the exposed fiber section is facilitated by the low emissivity of the transparent silica cladding compared to the silicon core. In Figure 15c, an intensity line scan along the fiber demonstrates the distinction between molten silicon and solid silicon based on their differing emissivities, with molten silicon exhibiting a clear dip in emissivity at the phase transition.

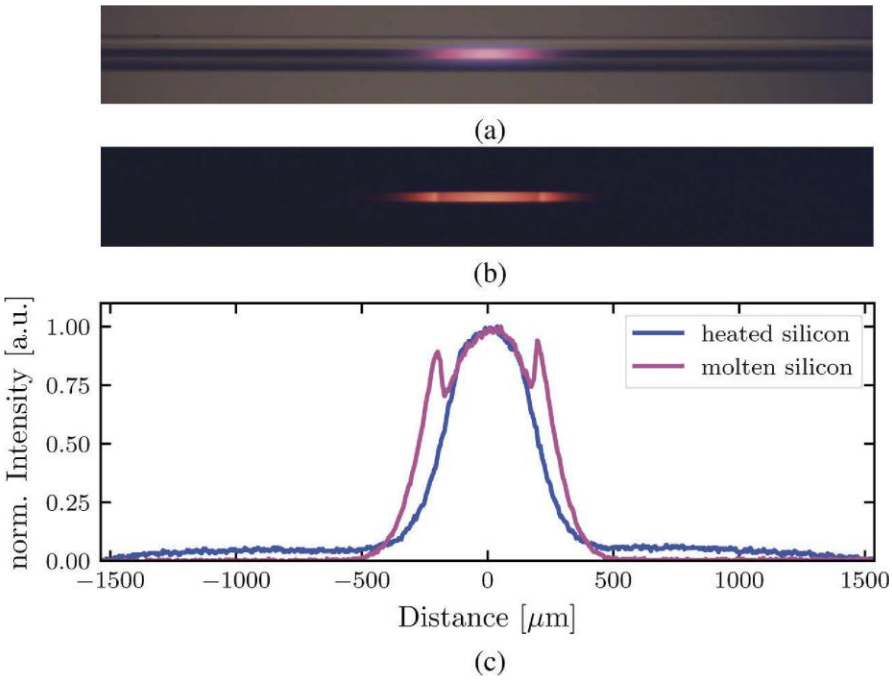

Figure 15. (**a**) Micrographs of a silicon core fiber (SCF) being heated by a CO_2 laser beam. (**b**) Micrograph of the same SCF heated at a higher laser power. (**c**) Intensity line scan along the fiber, illustrating the clear dip in emissivity at the phase transition between molten silicon and solid silicon [192].

Similarly, in [193], the flux-assisted molten core method was employed for laser post-processing on a ZnSe core infused with Cu8GeSe6. The extension of the molten core technique, introduced in [194], allowed the creation of glass-clad, crystalline gallium arsenide (GaAs) core fibers, a remarkable accomplishment given GaAs's challenges, with laser annealing to separate the Sn and GaAs phases. Lastly, the study in [195] demonstrated laser recrystallization following the thermal drawing of a fiber with a single-crystalline tellurium core.

Two-photon lithography (TPL) serves as a versatile additive manufacturing technology for creating 2D and 3D micro- and nanostructures with sub-wavelength resolution [196]. Usually, a tunable femtosecond laser is employed as the excitation source, operating in a working range of 690–1040 nm, with a pulse width of 140 fs and a pulse frequency of 80 MHz. Ti:Sapphire-based oscillators are considered ideal for TPL applications due to their ability to provide a broad range of available wavelengths with ultrashort pulses. Also, these lasers meet the requirements for high intensity and temporal precision needed to initiate two-photon processes. Recent advancements in laser technology have broadened the application of TPL-fabricated structures in microelectronics, photonics, optoelectronics, microfluidics, and plasmonic devices. In [197], research focused on the controlled precipitation of metallic nanostructures into glassy matrices, offering efficient synthesis for applications in photonics, optoelectronics, and telecommunications. The second, third, and fourth harmonic of a Q-switched Nd:YAG laser, operating at wavelengths of 532 nm, 355 nm, and 266 nm, respectively were utilized to perform the laser irradiation. The laser pulses had an energy of approximately 40 mJ, corresponding to an energy density per pulse of about 0.36 J/cm^2, and a duration of around 10 ns, with a pulse frequency of 2 Hz. Throughout the experiments, the pulse energy density remained constant, while the number of laser pulses varied. This was achieved through the modification of silver nanoparticles within silicate glasses and size control via post-exchange treatments such as thermal annealing and laser irradiation.

Thus, laser-processed smart materials represent a significant advancement in photonics and optoelectronics. Their ability to respond to external stimuli and adapt their optical properties offer new avenues for innovative photonic and optoelectronic devices, fostering more dynamic, efficient, and versatile technologies in these fields.

7. Computer-Generated Diffractive Optical Elements for Laser-Processed Smart Materials

Computer-generated DOEs hold significant promise for the manufacturing and modification of laser-processed materials [49]. They enable the precise shaping of material structures, leading to improvements in their physical and mechanical properties by laser modification [198–200]. DOEs are structures that introduce specific phase shifts into the incoming wave to create the desired phase profile of the outgoing beam [201]. They offer such advantages as high efficiency, precision, compact size, and flexibility, with two primary types: beam splitters and beam shapers. Beam splitters divide the laser beam into multiple beams, while beam shapers transform input beams into uniform spots of specific shapes. Figure 16 presents various diffractive structures demonstrating their capacity to redirect and divide incident radiation.

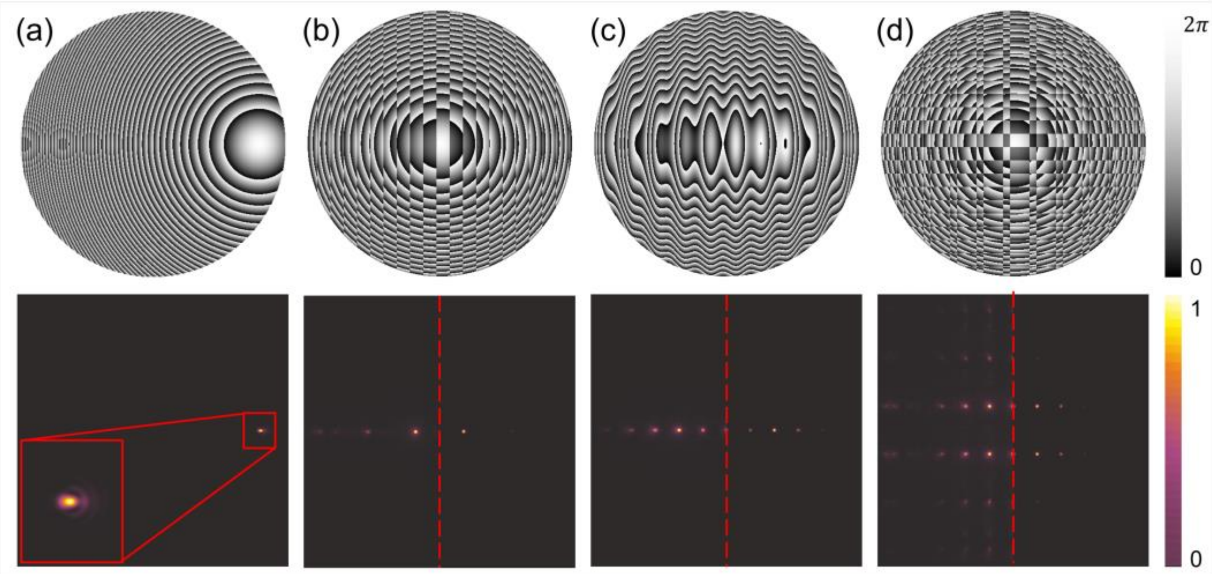

Figure 16. Illustration of diffractive structures. The upper panel shows phase delay maps for each structure, and the lower panel outlines intensity distribution in the focal plane. Symmetrical distributions are visualized in two halves, with the left corresponding to amplitude distribution and the right to intensity distribution. Structure (**a**) functions as a shifted lens, directing radiation away from the optical axis, with increased aberrations observed in the zoomed-in focal spot as the shift from the optical axis increases. Structure (**b**) combines a binary phase grating with a converging lens, creating two spots alongside the optical axis. Structure (**c**) pairs a sinusoidal phase grating with a converging lens, while structure (**d**) is a Dammann grating, forming a 3 × 2—point matrix joined with a converging lens [201].

Laser processing for smart materials often requires the accurate irradiation of specific surface areas with adjustable intensity. For example, in laser hardening of steels, it is necessary to achieve uniform martensitic transformation and avoid uneven superheating laser hardening of steels, it is necessary to achieve uniform martensitic transformation and avoid overheating non-uniformities. However, the use of laser beams with limited sizes provided by standard laser equipment typically requires the creation of multiple tracks, leading to issues with the uniformity of hardening. Various optical systems for shaping of laser beams have limited intensity adjustment capabilities, which hinder adaptation to the geometric features of processed objects and the required thermal cycles for the chosen material. The use of free-form DOEs allows for the dynamic adaptation of the laser beam, ensuring, when required, the relative uniformity of the hardened profile [202]. Such an approach includes solving the inverse heat conduction problem to achieve desired thermal effects in materials. The benefits of this approach are evident, particularly in enhancing temperature field parameters during laser heat treatment, including ensuring uniform temperature distribution. In the experimental phase of the study, chromium-nickel-molybdenum steel samples were processed using a CO_2 laser. The laser processing was carried out with varying the laser power between 800 and 1000 W, with a processing speed of 10–13 mm/s. The modified laser optical system was equipped with a DOE as the beam-focusing mirror. The laser beam was precisely focused to shape an approximately rectangular laser spot with a specified power density distribution. Additionally, the importance of integrating optical system components for real-time adjustments to the laser beam's shape and intensity has been emphasized.

A technique for laser local annealing of sheet aluminum and titanium alloys was formulated [203], expanding the potential for shaping these materials and improving the accuracy of structural component production. Titanium alloys, critical for durability in power and aerospace industries, encounter challenges in cold shaping due to high deformation resistance, hardening, and susceptibility to cracking. The utilization of computer-generated DOEs facilitates laser heating, the preferred method for creating local processing zones, significantly enhancing the properties of the pseudo-alpha titanium alloy Ti-2Al-1.5Mn [49]. The annealing zone exhibits a granular structure comprising the α-phase and a small amount of the β-phase. The fibrous structure formed by plastic deformation was eliminated through this laser annealing, forming a well-defined grain structure. The laser power was set at 450 W, and the processing speed is maintained at 6 mm/s. For redistribution of the power density in the focal spot of the laser beam, subsequently shaped by a DOE, a telescopic system consisting of two lenses was used. Figure 17 illustrates the microstructure of the cross-section of the Ti-2Al-1.5Mn rolled sheet titanium alloy after laser annealing. Research demonstrated that laser annealing augmented ultimate tensile strain and reduced the minimum bend angle for cold deformation, presenting opportunities to forming options for Ti-2Al-1.5Mn with higher accuracy and without additional heating.

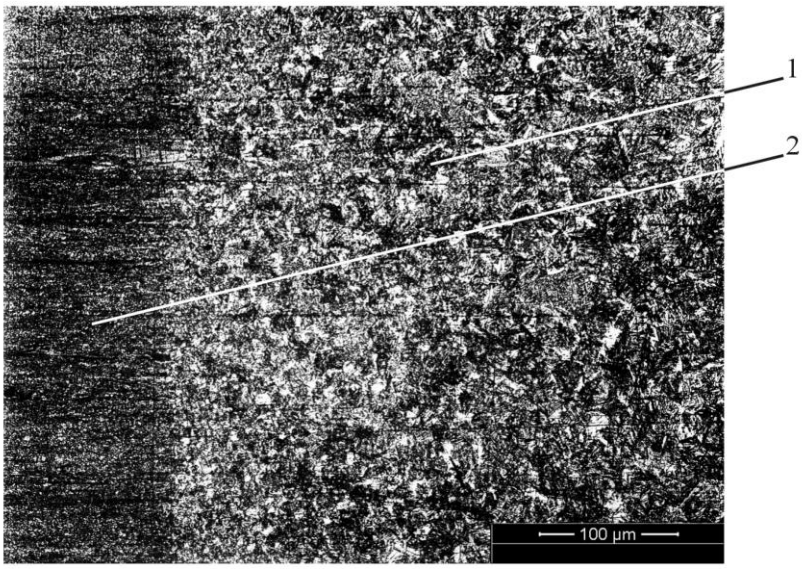

Figure 17. Microstructure of Ti-2Al-1.5Mn rolled sheet titanium alloy after laser annealing using DOEs, highlighting the annealing zone (1) and initial structure (2). Laser heating enhanced pseudo-alpha titanium alloy properties, fostering a granular structure with improved ultimate tensile strain and reduced minimum bend angle for cold deformation [49].

Computer-generated DOEs offer innovative possibilities for tailoring material characteristics and performance with exceptional precision. In this way, for example, their applications facilitate the development of more sensitive optical sensors for a wide range of applications, including medical diagnostics, environmental monitoring, and security technologies [204]. In [205], DOEs enabled high spatial multiplexing of femtosecond laser pulses with a sub-MHz repetition rate, showcasing a single-step, cost-effective, and versatile lithographic tool that does not require a mask. This advancement facilitated ultrahigh micropatterning rates and the creation of mm-sized surface-enhanced infrared absorption sensors. The experimental setup utilized fundamental-harmonic pulses generated by a laser with a central wavelength of 1030 nm and a duration of 300 fs. These pulses were generated with an energy of around 5 μJ and a frequency ranging from 0 to 2 MHz. The optical configuration included not only lenses and a galvanometric scanner but also a DOE made of fused silica.

An encouraging application of computer-generated DOEs involves the precise fabrication of nanostructures in the form of porous and oxide-metallic materials. Manipulating nanostructure morphology within specific regions of the laser-affected zone can be effectively addressed by modifying the laser beam's shape and redistributing its energy, particularly power density [206–208]. For the processing tasks, a CO_2 laser with diffusion cooling and radio frequency excitation was utilized. The laser generated pulses with durations ranging from 0.026 to 125 ms, and the average power of the laser beam was adjusted within the range of 200 W to 330 W. Using a laser beam modulated within the range of 3 Hz to 5 kHz, studies have revealed that the collaborative impact of thermal influences originating from laser pulses and laser-induced vibrations, specifically within the sound frequency spectrum, leads to a significant enhancing in the diffusion coefficient within materials. The crucial element for enhancing mass transfer in the solid phase of metallic materials, whether of the heated in an oxidation-free environment or selectively oxidable metallic materials, was recognized as the dynamic stress–strain state caused by laser-induced vibrations.

This innovative approach involves the use of computer-generated DOEs for shaping the laser beam, enhancing the precision of energy transmission onto material surfaces, even those with intricate shapes. It opens up avenues for exploration and innovation, including laser processing to reduce the friction coefficient of silicon carbide ceramics [209]. DOEs employ micro-scaled relief for changing the phase of the light wave, allowing us to control the light intensity profiles in various applications. DOEs find applications in laser material processing, microscopy, and scientific fields, offering solutions for different wavelengths, beam sizes, and working distances [210]. Exploring computer-synthesized diffractive optical elements for laser processing, the study in [211] showcased enhanced material properties, including improved hardness, wear resistance, and weld strength, achieved through precise control of spatial beam power distribution.

The utilization of computer-generated DOEs shows great promise for precision engineering and offers solutions for crafting nanostructures in diverse materials. They enable meticulous control over the spatial distribution of laser energy, making them a valuable asset in enhancing smart material performance and characteristics across various industrial sectors. The potential for ongoing research and practical applications in this field is expanding, indicating good prospects for the near future.

8. Conclusions

Laser processing enhances smart materials, enabling adaptive transformations for a wide range of industries. This modern approach to enhancing material intelligence enables the creation of surface modifications, atomically thin materials, and micro- and nanostructures, offering the potential for self-cleaning surfaces and improved thermoelectric performance in metals. Laser irradiation and processing also facilitate the development of shape memory materials, the introduction of functional additives, and the creation of MEMS with adaptive properties, impacting diverse fields such as medicine, electronics, aerospace, and photonics. This promising area of research aims to harness laser processing to address various challenges, with the potential to revolutionize multiple industrial sectors by creating smart materials with enhanced adaptability and intelligent functions.

Laser modification is a versatile technique for changing the properties of materials, offering precision and customization in shaping their surface characteristics, making it an essential tool for applications in medicine, electronics, engineering, and biotechnology. It enables the creation of smart materials by selectively adjusting material surfaces, preserving their bulk properties, and achieving targeted modifications. This method is highly customizable, suitable for a wide range of materials, and is used in diverse fields, promising innovative solutions with adaptive surface properties for technological advances and contemporary challenges.

Laser modification, encompassing photothermal reactions and functional additive integration, enables precise control and customization of material properties, facilitating adaptability for diverse applications. Photothermal reactions, driven by localized laser heating, induce structural and property changes in materials. Functional additives, including polymers, nanoparticles, and metals, enhance materials with new properties and functionalities, finding utility in electronics, aerospace, medicine, and environmental monitoring.

DLIP, utilizing coherent laser beam interference, stands out as an exceptionally versatile and rapid method for crafting large-scale defect-free micro- and nanostructures on surfaces, finding diverse applications, encompassing electrical, optical, and tribological domains. The distinctive feature of the method, not requiring focused laser beams, enables high-performance processing with a substantial depth of focus, making DLIP a potent and efficient technique for modifying surface properties across diverse technological applications. This method has been successfully implemented using different pulsed laser sources, processing systems and con-figurations for a wide range of materials. DLIP applications open new perspectives for fabrication of multifunctional surfaces for advanced applications.

The combination of laser processing and smart materials has become the basis for 4D printing, which allows objects to change shape or function depending on external influences. Shape memory materials, including shape memory alloys and polymers, play a pivotal role in this technology, offering a wide range of possibilities for applications in the aerospace, robotics, health care, consumer electronics, and automotive industries. The versatility and adaptability of these materials make them a promising avenue for innovation and advancement in various sectors.

Laser processing of smart materials opens up new opportunities in photonics and optoelectronics, enabling precise control over the optical properties of materials and facilitating the development of responsive devices. In photonics, it has led to the creation of programmable photonic devices through laser-induced phase changes and nanostructuring, offering potential applications in fields like all-optical neural networks and photonic integrated circuits. In optoelectronics, laser processing is instrumental in engineering materials capable of dynamically adjusting their optical characteristics, enhancing the performance of devices such as LEDs and displays. These advancements significantly impact various applications, including the fabrication of photonic integrated circuits, improved solar cell efficiency, the production of LEDs with quantum dots for displays, optical fiber manufacturing, and two-photon lithography, ultimately shaping a more dynamic, efficient, and versatile future for photonics and optoelectronics.

Computer-generated DOEs provide precise control over laser beam power density, which enhances the precision of laser-based material manufacturing and modification. This technology provides the possibility of creating predetermined temperature distribution and allows real-time adjustments to the laser beam's shape and intensity, effectively overcoming existing limitations in optical systems. These advancements hold substantial potential for enhancing material properties in laser processing for smart materials. Briefly described are laser processing technologies and nanotechnologies using diffractive optical elements: laser local annealing of aluminum and titanium alloy sheets, enhancement of coating adhesion strength, reduction of friction coefficient in silicon carbide ceramics, selective modification of dual-phase steels, as well as precise fabrication of nanostructures in the form of porous and oxide-metallic materials. In the area of photonics and optoelectronics, these elements act as innovative tools, facilitating the development of adaptive materials with dynamically alterable optical characteristics, enabling the creation of intelligent optical devices and metamaterials, and promoting advances in 3D printing and microfabrication technologies.

The expanding potential for continued research and practical applications in this field suggests highly favorable prospects in the near future.

Author Contributions: Conceptualization, S.P.M.; methodology, S.P.M.; software, S.P.M. and C.S.; validation, S.P.M. and C.S.; formal analysis, S.P.M. and C.S.; investigation, S.P.M. and C.S.; resources, S.P.M. and C.S.; data curation, S.P.M. and C.S.; writing—original draft preparation, S.P.M.; writing—review and editing, S.P.M.; visualization, S.P.M. and C.S.; supervision, S.P.M. and C.S.; project administration, S.P.M. All authors have read and agreed to the published version of the manuscript.

Funding: This research received no external funding.

Data Availability Statement: Not applicable.

Conflicts of Interest: The authors declare no conflict of interest.

References

1. Xia, Y.; He, Y.; Zhang, F.; Liu, Y.; Leng, J. A review of shape memory polymers and composites: Mechanisms, materials, and applications. *Adv. Mater.* **2021**, *33*, 2000713. [CrossRef] [PubMed]
2. Akbar, I.; El Hadrouz, M.; El Mansori, M.; Lagoudas, D. Toward enabling manufacturing paradigm of 4D printing of shape memory materials: Open literature review. *Eur. Polym. J.* **2022**, *168*, 111106. [CrossRef]
3. Chen, X.; Hu, Z.; Lyu, Q.; Li, M.; Zhang, L.; Zhu, J. Shape memory photonic materials: Fabrication and emerging applications. *J. Mater. Chem. C* **2023**, *11*, 12466–12485. [CrossRef]
4. Ganeson, K.; Tan Xue May, C.; Abdullah, A.A.A.; Ramakrishna, S.; Vigneswari, S. Advantages and prospective implications of smart materials in tissue engineering: Piezoelectric, shape memory, and hydrogels. *Pharmaceutics* **2023**, *15*, 2356. [CrossRef] [PubMed]
5. Kulagin, I.; Li, M.; Laitinen, V.; Handroos, H. Review of MSM actuators: Applications, challenges, and potential. *IEEE Access* **2022**, *10*, 83841–83850. [CrossRef]
6. Van Vilsteren, S.J.M.; Yarmand, H.; Ghodrat, S. Review of magnetic shape memory polymers and magnetic soft materials. *Magnetochemistry* **2021**, *7*, 123. [CrossRef]
7. Barta, N.E.; Fincher, C.; Bolon, A.M.; Attari, V.; Higgins, W.; Arroyave, R.; Radovic, M.; Pharr, G.M.; Karaman, I. Fabrication and characterization of aluminum—magnetic shape memory alloy composites. *Mater. Sci. Eng. A* **2021**, *805*, 140549. [CrossRef]
8. Shahbazi, M.; Jäger, H.; Ettelaie, R.; Mohammadi, A.; Asghartabar Kashi, P. Multimaterial 3D printing of self-assembling smart thermo-responsive polymers into 4D printed objects: A review. *Addit. Manuf.* **2023**, *71*, 103598. [CrossRef]
9. Wang, B.; Patkar, S.S.; Kiick, K.L. Application of thermoresponsive intrinsically disordered protein polymers in nanostructured and microstructured materials. *Macromol. Biosci.* **2021**, *21*, 2100129. [CrossRef]
10. Archimi, M.; Schoolaert, E.; Becelaere, J.; Hoogenboom, R.; Camposeo, A.; De Clerck, K.; Pisignano, D. Optical gain switching by thermo-responsive light-emitting nanofibers through moisture sorption swelling. *Adv. Opt. Mater.* **2023**, *11*, 2202056. [CrossRef]
11. Ahn, J.; Gu, J.; Choi, J.; Jeong, Y.; Park, J.; Cho, S.; Oh, Y.S.; Jeong, J.-H.; Amjadi, M.; Park, I. A review of recent advances in electrically driven polymer-based flexible actuators: Smart materials, structures, and their applications. *Adv. Mater. Technol.* **2022**, *7*, 2200041. [CrossRef]
12. Palza, H.; Zapata, P.A.; Angulo-Pineda, C. Electroactive smart polymers for biomedical applications. *Materials* **2019**, *12*, 277. [CrossRef] [PubMed]
13. Kamely, N. Interaction of light with different electroactive materials: A review. *J. Electron. Mater.* **2022**, *51*, 953–965. [CrossRef]
14. Shen, W.; Li, G. Recent progress in liquid crystal-based smart windows: Materials, structures, and design. *Laser Photonics Rev.* **2023**, *17*, 2200207. [CrossRef]
15. Kim, M.-S.; Heo, J.-K.; Rodrigue, H.; Lee, H.-T.; Pané, S.; Han, M.-W.; Ahn, S.-H. Shape memory alloy (SMA) actuators: The role of material, form, and scaling effects. *Adv. Mater.* **2023**, *35*, 2208517. [CrossRef] [PubMed]
16. Kannatey-Asibu, E., Jr. *Principles of Laser Materials Processing: Developments and Applications*, 2nd ed.; John Wiley & Sons: Hoboken, NJ, USA, 2023; 608p.
17. Sasi, R.; Kanmani Subbu, S.; Palani, I.A. Performance of laser surface textured high speed steel cutting tool in machining of Al7075-T6 aerospace alloy. *Surf. Coat. Technol.* **2017**, *313*, 337–346. [CrossRef]
18. Riveiro, A.; Quintero, F.; Boutinguiza, M.; del Val, J.; Comesana, R.; Lusquiños, F.; Pou, J. Laser cutting: A review on the influence of assist gas. *Materials* **2019**, *12*, 157. [CrossRef]
19. Sharma, A.; Yadava, V. Experimental analysis of Nd-YAG laser cutting of sheet materials—A review. *Opt. Laser Technol.* **2018**, *98*, 264–280. [CrossRef]
20. Biffi, C.A.; Fiocchi, J.; Tuissi, A. Relevant aspects of laser cutting of NiTi shape memory alloys. *J. Mater. Res. Technol.* **2022**, *19*, 472–506. [CrossRef]

21. Milosavljevic, D.; Caprio, L.; Busatto, M.; Cinquemani, S.; Lecis, N.; Previtali, B. Effects of laser cutting on the chemical composition and phase transformation capacity in Cu-Al-Mn shape memory alloy sheets. *Proc. SPIE* **2023**, *12483*, 124830P.
22. Lanzilotti, C.O.; Pinto, L.F.R. Laser engraving for product traceability: Advances toward sustainable manufacturing. *J. Environ. Account. Manag.* **2022**, *10*, 203–214. [CrossRef]
23. Klimenda, F.; Sterba, J.; Cernohlavek, V.; Ponikelsky, J.; Maran, P. Draft of robotic workstation for laser engraving. *Manuf. Technol.* **2021**, *21*, 357–363. [CrossRef]
24. Liu, Z.; Li, X.; Pan, L.; Gao, J.; Zhang, K. Effects of weld penetration modes on laser welding characteristics of a novel ultra-high strength steel for aerospace application. *J. Manuf. Process.* **2023**, *90*, 111–124. [CrossRef]
25. He, S.; Chen, S.; Zhao, Y.; Qi, N.; Zhan, X. Study on the intelligent model database modeling the laser welding for aerospace aluminum alloy. *J. Manuf. Process.* **2021**, *63*, 121–129. [CrossRef]
26. Wen, P.; Yelkenci, D.; Chen, J.; Chang, B.; Du, D.; Shan, J. Numerical analysis of the effect of welding positions on formation quality during laser welding of TC4 titanium alloy parts in aerospace industry. *J. Laser Appl.* **2019**, *31*, 022401. [CrossRef]
27. Bassani, P.; Fiocchi, J.; Tuissi, A.; Biffi, C.A. Investigation of the effect of laser fluence on microstructure and martensitic transformation for realizing functionally graded NiTi shape memory alloy via laser powder bed fusion. *Appl. Sci.* **2023**, *13*, 882. [CrossRef]
28. Meyer, R.; Stock, F.; Antoni, F.; Hajjar-Garreau, S.; Muller, D. Investigation of laser-induced changes in structural and optoelectrical properties of pulsed laser-deposited diamond-like carbon layers. *J. Mater. Sci. Mater. Electron.* **2023**, *34*, 1368. [CrossRef]
29. Zhang, X.; Walmsley, T.S.; Xu, Y.-Q. In situ monitoring of electrical and optoelectronic properties of suspended graphene ribbons during laser-induced morphological changes. *Nanoscale Adv.* **2020**, *2*, 4034–4040. [CrossRef]
30. Arulvel, S.; Rufuss, D.D.W.; Jain, A.; Kandasamy, J.; Singhal, M. Laser processing techniques for surface property enhancement: Focus on material advancement. *Surf. Interfaces* **2023**, *42*, 103293.
31. Xiao, K.; Geohegan, D.B. Laser synthesis and processing of atomically thin 2D materials. *Trends Chem.* **2022**, *4*, 769–772. [CrossRef]
32. Wang, H.; Wang, Q.; Huo, L.; Liu, J.; Bai, Z. High-efficient laser-based bionic surface structuring for enhanced surface functionalization and self-cleaning effect. *Surf. Interfaces* **2023**, *37*, 102691. [CrossRef]
33. Srin, K.S.; Ramkumar, J.; Bathe, R. The isotropic and anisotropic self-cleaning surfaces by using only femtosecond laser. *Results Mater.* **2023**, *17*, 100362. [CrossRef]
34. Wan, Y.; Wang, X.; Zhang, C.; Xu, J. Durable self-cleaning hydrophobic surface of hollow cylindrical stainless steel with controllable adhesion prepared by nanosecond laser. *Vacuum* **2022**, *205*, 111422. [CrossRef]
35. Gomell, L.; Haeger, T.; Roscher, M.; Bishara, H.; Heiderhoff, R.; Riedl, T.; Scheu, C.; Gault, B. Microstructure manipulation by laser-surface remelting of a full-Heusler compound to enhance thermoelectric properties. *Acta Mater.* **2022**, *223*, 117501. [CrossRef]
36. Zhao, F.; Rong, W.; Wang, L.; Sun, L. Photothermal-responsive shape-memory magnetic helical microrobots with programmable addressable shape changes. *ACS Appl. Mater. Interfaces* **2023**, *15*, 25942–25951. [CrossRef] [PubMed]
37. Schuleit, M.; Theren, B.; Maack, P.; Kuhlenkötter, B.; Esen, C. Investigation of minimal strokes of NiTi shape memory wires using laser activation. *Procedia CIRP* **2020**, *94*, 542–545. [CrossRef]
38. Seiler, M.; Knauft, A.; Gruben, J.J.; Frank, S.; Barz, A.; Bliedtner, J.; Lasagni, A.F. Modification of polymeric surfaces with ultrashort laser pulses for the selective deposition of homogeneous metallic conductive layers. *Materials* **2022**, *15*, 6572. [CrossRef]
39. Norouzi, M.H.; Weber, J.; Tesmann, C.; Lohmuller, E.; Lohmuller, S.; Saint-Cast, P.; Hofmann, M. PERC Solar cells on p-type Cz-Si utilizing phosphorus-doped SiNXlayers. *IEEE J. Photovolt.* **2022**, *12*, 213–221. [CrossRef]
40. Vaqueiro-Contreras, M.; Hallam, B.; Chan, C. Review of laser doping and its applications in silicon solar cells. *IEEE J. Photovolt.* **2023**, *13*, 373–384. [CrossRef]
41. Greenberg, E.; Armon, N.; Kapon, O.; Ben-Ishai, M.; Shpaisman, H. Nanostructure and mechanism of metal deposition by a laser-induced photothermal reaction. *Adv. Mater. Interfaces* **2019**, *6*, 1900541. [CrossRef]
42. Guseva, O.S.; Kozlov, D.V.; Korpukhin, A.S.; Smirnov, I.P.; Andreev, P.A. Application of a femtosecond laser in the fabrication of quartz sensing elements for MEMS accelerometers. *Nanobiotechnol. Rep.* **2022**, *17*, S4–S8. [CrossRef]
43. Ge, C.; Cretu, E. Simple and robust microfabrication of polymeric piezoelectric resonating MEMS mass sensors. *Sensors* **2022**, *22*, 2994. [CrossRef]
44. Meléndez-Campos, J.; Vázquez-Piñón, M.; Camacho-Leon, S. Sensitivity analysis of a portable wireless pcb-mems permittivity sensor node for non-invasive liquid recognition. *Micromachines* **2021**, *12*, 1068. [CrossRef] [PubMed]
45. Balčas, G.; Malinauskas, M.; Farsari, M.; Juodkazis, S. Fabrication of glass-ceramic 3D micro-optics by combining laser lithography and calcination. *Adv. Funct. Mater.* **2023**, *33*, 2215230. [CrossRef]
46. Jia, Y.; Chen, F. Recent progress on femtosecond laser micro-/nano-fabrication of functional photonic structures in dielectric crystals: A brief review and perspective. *APL Photonics* **2023**, *8*, 090901. [CrossRef]
47. Li, J.; Cao, C.; Qiu, Y.; Kuang, C.; Liu, X. Optical waveguides fabricated via femtosecond direct laser writing: Processes, materials, and devices. *Adv. Mater. Technol.* **2023**, *8*, 2300620. [CrossRef]
48. Zhao, L.; Liu, Z.; Chen, D.; Liu, F.; Yang, Z.; Li, X.; Yu, H.; Liu, H.; Zhou, W. Laser synthesis and microfabrication of micro/nanostructured materials toward energy conversion and storage. *Micro Nano Lett.* **2021**, *13*, 49. [CrossRef]
49. Murzin, S.P.; Kazanskiy, N.L.; Stiglbrunner, C. Analysis of the advantages of laser processing of aerospace materials using diffractive optics. *Metals* **2021**, *11*, 963. [CrossRef]
50. Yao, J.; Zhang, Q.; Liu, R.; Wu, G. *Laser Applications in Surface Modification*; Springer: Singapore, 2022; 151p.

51. Masood Bukhari, S.; Husnain, N.; Arsalan Siddiqui, F.; Tuoqeer Anwar, M.; Abbas Khosa, A.; Imran, M.; Hassan Qureshi, T.; Ahmad, R. Effect of laser surface remelting on microstructure, mechanical properties and tribological properties of metals and alloys: A review. *Opt. Laser Technol.* **2023**, *165*, 109588. [CrossRef]
52. Slobodyan, M.; Pesterev, E.; Markov, A. A review of high-energy processing techniques applied for additive manufacturing and surface engineering of cemented carbides and cermets. *J. Manuf. Process.* **2023**, *105*, 124–186. [CrossRef]
53. Arakelian, S.M.; Evstyunin, G.A.; Zdanov, A.V.; Abrakhin, S.I. Modern laser-technologies and nanotechnologies—Next-generation on new physical principles. *J. Phys. Conf. Ser.* **2021**, *2131*, 052081. [CrossRef]
54. Stratakis, E.; Bonse, J.; Heitz, J.; Siegel, J.; Tsibidis, G.D.; Skoulas, E.; Papadopoulos, A.; Mimidis, A.; Joel, A.-C.; Comanns, P.; et al. Laser engineering of biomimetic surfaces. *Mater. Sci. Eng. R Rep.* **2020**, *141*, 100562. [CrossRef]
55. Tong, W.; Xiong, D. Direct laser texturing technique for metal surfaces to achieve superhydrophobicity. *Mater. Today Phys.* **2022**, *23*, 100651. [CrossRef]
56. Emelyanenko, K.A.; Emelyanenko, A.M.; Boinovich, L.B. Laser obtained superhydrophobic state for stainless steel corrosion protection, a review. *Coatings* **2023**, *13*, 194. [CrossRef]
57. Deng, W.; Wang, C.; Lu, H.; Meng, X.; Wang, Z.; Lv, J.; Luo, K.; Lu, J. Progressive developments, challenges and future trends in laser shock peening of metallic materials and alloys: A comprehensive review. *Int. J. Mach. Tools Manuf.* **2023**, *191*, 104061. [CrossRef]
58. Singh, S.N.; Deoghare, A.B. Laser shock peening of laser based directed energy deposition and powder bed fusion additively manufactured parts: A review. *Met. Mater. Int.* **2023**, *29*, 1563–1585. [CrossRef]
59. Liu, J.; Ye, C.; Dong, Y. Recent development of thermally assisted surface hardening techniques: A review. *Adv. Ind. Manuf. Eng.* **2021**, *2*, 100006. [CrossRef]
60. Marimuthu, P. Status of laser transformation hardening of steel and its alloys: A review. *Emerg. Mater. Res.* **2019**, *8*, 188–205.
61. Ren, D.; Zhang, P.; Yu, J.; Yao, Y.; Li, X. Study on the quenching depth and surface hardness of metal materials by laser quenching variable parameters. *Front. Phys.* **2023**, *10*, 1115447. [CrossRef]
62. Radkiewicz, P.; Laurentowski, M.; Reiner, J. Improvement of laser hardening technology with oscillating beam using multiphysics simulation. *Procedia CIRP* **2022**, *111*, 557–561. [CrossRef]
63. Aprilia, A.; Maharjan, N.; Zhou, W. Decarburization in laser surface hardening of AISI 420 martensitic stainless steel. *Materials* **2023**, *16*, 939. [CrossRef] [PubMed]
64. Siddiqui, A.A.; Dubey, A.K. Recent trends in laser cladding and surface alloying. *Opt. Laser Technol.* **2021**, *134*, 106619. [CrossRef]
65. Mosallanejad, M.H.; Niroumand, B.; Aversa, A.; Saboori, A. In-situ alloying in laser-based additive manufacturing processes: A critical review. *J. Alloys Compd.* **2021**, *872*, 159567. [CrossRef]
66. Han, T.; Zhou, K.; Chen, Z.; Gao, Y. Research progress on laser cladding alloying and composite processing of steel materials. *Metals* **2022**, *12*, 2055. [CrossRef]
67. Škamat, J.; Bučelis, K.; Černašėjus, O.; Indrišiūnas, S. Fiber laser alloying of additively manufactured 18Ni-300 maraging steel part surface: Effect of processing parameters on the formation of alloyed surface layer and its properties. *Materials* **2023**, *16*, 4732. [CrossRef] [PubMed]
68. Huet, K.; Mazzamuto, F.; Tabata, T.; Toque-Tresonne, I.; Mori, Y. Doping of semiconductor devices by laser thermal annealing. *Mater. Sci. Semicond. Process.* **2017**, *62*, 92–102. [CrossRef]
69. Pyo, J.; Lee, B.; Ryu, H.-Y. Evaluation of crystalline volume fraction of laser-annealed polysilicon thin films using raman spectroscopy and spectroscopic ellipsometry. *Micromachines* **2021**, *12*, 999. [CrossRef] [PubMed]
70. Khairullina, E.M.; Ratautas, K.; Panov, M.S.; Andriianov, V.S.; Mickus, S.; Manshina, A.A.; Račiukaitis, G.; Tumkin, I.I. Laser-assisted surface activation for fabrication of flexible non-enzymatic Cu-based sensors. *Mikrochim. Acta* **2022**, *189*, 259. [CrossRef]
71. Seiler, M.; Gruben, J.; Knauft, A.; Barz, A.; Bliedtner, J. Laser beam activation of polymer surfaces for selective chemical metallization. *Procedia CIRP* **2020**, *94*, 891–894. [CrossRef]
72. Tyuftin, A.A.; Kerry, J.P. Review of surface treatment methods for polyamide films for potential application as smart packaging materials: Surface structure, antimicrobial and spectral properties. *Food Packag. Shelf Life* **2020**, *24*, 100475. [CrossRef]
73. Sirdeshmukh, N.; Dongre, G. Laser micro & nano surface texturing for enhancing osseointegration and antimicrobial effect of biomaterials: A review. *Mater. Today Proc.* **2021**, *44*, 2348–2355.
74. Omarov, S.; Nauryz, N.; Talamona, D.; Perveen, A. Surface modification techniques for metallic biomedical alloys: A concise review. *Metals* **2023**, *13*, 82. [CrossRef]
75. Vidyasagar, K.E.C.; Aggarwal, V.; Sinha, S.S.; Saha, S.K.; Kalyanasundaram, D. Laser based micro texturing of freeform surfaces of implants using a Stewart platform. *Precis. Eng.* **2021**, *72*, 294–303. [CrossRef]
76. Wang, L.; Zhao, Y.; Yang, Y.; Pang, X.; Hao, L.; Zhao, Y.; Liu, J. Development of laser-micromachined 4H-SiC MEMS piezoresistive pressure sensors for corrosive environments. *IEEE Trans. Electron Devices* **2022**, *69*, 2009–2014. [CrossRef]
77. Linden, J.; Melech, N.; Sakaev, I.; Fogel, O.; Krylov, S.; Nuttman, D.; Zalevsky, Z.; Sirota, M. Femtosecond laser-assisted fabrication of piezoelectrically actuated crystalline quartz-based MEMS resonators. *Microsyst. Nanoeng.* **2023**, *9*, 38. [CrossRef]
78. Yu, X.; Yasunaga, Y.; Goto, K.; Liu, D.; Ono, S. Profile control of femtosecond laser-fabricated moth-eye structures on Si substrate. *Opt. Lasers Eng.* **2021**, *142*, 106584. [CrossRef]
79. Wang, H.; Zhang, F.; Yin, K.; Duan, J. Bioinspired antireflective subwavelength nanostructures induced by femtosecond laser for high transparency glass. *J. Non-Cryst. Solids* **2023**, *600*, 122016. [CrossRef]

80. Ren, X.; Zou, H.; Diao, Q.; Wang, C.; Wang, Y.; Li, H.; Sui, T.; Lin, B.; Yan, S. Surface modification technologies for enhancing the tribological properties of cemented carbides: A review. *Tribol. Int.* **2023**, *180*, 108257. [CrossRef]
81. Mao, B.; Siddaiah, A.; Liao, Y.; Menezes, P.L. Laser surface texturing and related techniques for enhancing tribological performance of engineering materials: A review. *J. Manuf. Process.* **2020**, *53*, 153–173. [CrossRef]
82. Lazov, L.; Teirumnieks, E.; Angelov, N.; Yankov, E. Modification of the roughness of 304 stainless steel by laser surface texturing (LST). *Laser Phys.* **2023**, *33*, 046001. [CrossRef]
83. Barimah, E.K.; Boontan, A.; Steenson, D.P.; Jose, G. Infrared optical properties modulation of VO_2 thin film fabricated by ultrafast pulsed laser deposition for thermochromic smart window applications. *Sci. Rep.* **2022**, *12*, 11421. [CrossRef] [PubMed]
84. Um, S.-H.; Hwang, S.-W.; Grigoropoulos, C.P.; Jeon, H.; Ko, S.H. Recent advances in selective laser-material interaction for biomedical device applications. *Appl. Phys. Rev.* **2022**, *9*, 041302. [CrossRef]
85. Ali, B.; Litvinyuk, I.V.; Rybachuk, M. Femtosecond laser micromachining of diamond: Current research status, applications and challenges. *Carbon* **2021**, *179*, 209–226. [CrossRef]
86. Huang, J.; Liu, Y.; Jin, S.; Wang, Z.; Qi, Y.; Zhang, J.; Wang, K.; Qiu, R. Uniformity control of laser-induced periodic surface structures. *Front. Phys.* **2022**, *10*, 932284. [CrossRef]
87. Sypniewska, J.; Szkodo, M. Influence of laser modification on the surface character of biomaterials: Titanium and its alloys—A review. *Coatings* **2022**, *12*, 1371. [CrossRef]
88. Museur, L.; Manousaki, A.; Anglos, D.; Tsibidis, G.D.; Kanaev, A. Pathways control in modification of solid surfaces induced by temporarily separated femtosecond laser pulses. *Appl. Surf. Sci.* **2021**, *566*, 150611. [CrossRef]
89. Al Harbi, N.; Benyounis, K.Y.; Looney, L.; Stokes, J. Laser Surface Modification of Ceramic Coating Materials. In *Encyclopedia of Smart Materials*, 1st ed.; Olabi, A.-G., Ed.; Elsevier: Amsterdam, The Netherlands, 2018; pp. 445–461.
90. Hong, S.; Lee, H.; Yeo, J.; Ko, S.H. Digital selective laser methods for nanomaterials: From synthesis to processing. *Nano Today* **2016**, *11*, 547–564. [CrossRef]
91. Haine, A.T.; Niidome, T. Gold nanorods as nanodevices for bioimaging, photothermal therapeutics, and drug delivery. *Chem. Pharm. Bull.* **2017**, *65*, 625–628. [CrossRef]
92. Wu, C.Y.; Rong, Y.M.; Huang, Y.; Zhang, G.J. Laser cutting of thermoplastic film: Mechanism and processing technology. *Sci. China Technol. Sci.* **2022**, *65*, 2068–2078. [CrossRef]
93. Jia, X.; Chen, Y.; Liu, L.; Wang, C.; Duan, J. Advances in laser drilling of structural ceramics. *Nanomaterials* **2022**, *12*, 230. [CrossRef]
94. Siddharth, S.; Chen, Y.-B.; Lee, M.-T. Transport phenomena of bubble growth coupled with chemical reaction during laser-induced photothermal reduction and deposition processes. *Int. J. Heat Mass Transf.* **2023**, *216*, 124550. [CrossRef]
95. Joe, D.J.; Kim, S.; Park, J.H.; Park, D.Y.; Lee, H.E.; Im, T.H.; Choi, I.; Ruoff, R.S.; Lee, K.J. Laser–material interactions for flexible applications. *Adv. Mater.* **2017**, *29*, 1606586. [CrossRef] [PubMed]
96. Ramon, J.; Xiong, R.; De Smedt, S.C.; Raemdonck, K.; Braeckmans, K. Vapor nanobubble-mediated photoporation constitutes a versatile intracellular delivery technology. *Curr. Opin. Colloid Interface Sci.* **2021**, *54*, 101453. [CrossRef]
97. Yamada, Y.; Takano, Y.; Satrialdi; Abe, J.; Hibino, M.; Harashima, H. Therapeutic strategies for regulating mitochondrial oxidative stress. *Biomolecules* **2020**, *10*, 83. [CrossRef] [PubMed]
98. Liu, Y.; Wang, K.; Fu, H. Improvement of the high temperature wear resistance of laser cladding nickel-based coating: A review. *Metals* **2023**, *13*, 840. [CrossRef]
99. Zhao, H.; Zhao, C.; Xie, W.; Wu, D.; Du, B.; Zhang, X.; Wen, M.; Ma, R.; Li, R.; Jiao, J.; et al. Research progress of laser cladding on the surface of titanium and its alloys. *Materials* **2023**, *16*, 3250. [CrossRef] [PubMed]
100. Liu, B.; Deng, Z.; Liu, D. Preparation and properties of multilayer Ca/P bio-ceramic coating by laser cladding. *Coatings* **2021**, *11*, 891. [CrossRef]
101. Liang, Y.; Liao, Z.Y.; Zhang, L.L.; Cai, M.W.; Wei, X.S.; Shen, J. A review on coatings deposited by extreme high-speed laser cladding: Processes, materials, and properties. *Opt. Laser Technol.* **2023**, *164*, 109472. [CrossRef]
102. Raj, D.; Maity, S.R.; Das, B. State-of-the-art review on laser cladding process as an in-situ repair technique. *Proc. Inst. Mech. Eng. E J. Process Mech. Eng.* **2022**, *236*, 1194–1215. [CrossRef]
103. Li, M.; Huang, K.; Yi, X. Crack formation mechanisms and control methods of laser cladding coatings: A review. *Coatings* **2023**, *13*, 1117. [CrossRef]
104. Shen, X.; Peng, H.; Xue, Y.; Wang, B.; Su, G.; Zhu, J.; Li, A. Microstructure and Properties of WC/Ni-Based Laser-Clad Coatings with Different WC Content Values. *Materials* **2022**, *15*, 6309. [CrossRef] [PubMed]
105. Zhang, P.; Pang, Y.; Yu, M. Effects of WC particle types on the microstructures and properties of WC-Reinforced Ni60 composite coatings produced by laser cladding. *Metals* **2019**, *9*, 583. [CrossRef]
106. Liu, Y.; Ding, Y.; Yang, L.; Sun, R.; Zhang, T.; Yang, X. Research and progress of laser cladding on engineering alloys: A review. *J. Manuf. Process.* **2021**, *66*, 341–363. [CrossRef]
107. Wang, K.; Liu, W.; Hong, Y.; Sohan, H.S.; Tong, Y.; Hu, Y.; Zhang, M.; Zhang, J.; Xiang, D.; Fu, H.; et al. An overview of technological parameter optimization in the case of laser cladding. *Coatings* **2023**, *13*, 496. [CrossRef]
108. Wei, R.; Ouyang, C.; Wang, R.; Zhao, C.; Li, H.; Deng, R. Research status of the transition layer on laser cladding. *Metall. Res. Technol.* **2023**, *120*, 318. [CrossRef]

109. Morake, J.B.; Mutua, J.M.; Ruthandi, M.M.; Olakanmi, E.O. The potential use of laser cladded functionally graded materials to mitigate degradation in boiler tube heat exchangers for power plant applications: A review. *Surf. Eng.* **2023**, *39*, 677–721. [CrossRef]
110. Cheng, W.; Ji, L.; Zhang, L.; Wang, H.; Sun, W. Refractory high-entropy alloys fabricated using laser technologies: A concrete review. *J. Mater. Res. Technol.* **2023**, *24*, 7497–7524. [CrossRef]
111. Zhou, J.-L.; Cheng, Y.-H.; Chen, Y.-X.; Liang, X.-B. Composition design and preparation process of refractory high-entropy alloys: A review. *Int. J. Refract. Met. Hard Mater.* **2022**, *105*, 105836. [CrossRef]
112. Arif, Z.U.; Khalid, M.Y.; Al Rashid, A.; ur Rehman, E.; Atif, M. Laser deposition of high-entropy alloys: A comprehensive review. *Opt. Laser Technol.* **2022**, *145*, 107447. [CrossRef]
113. Arif, Z.U.; Khalid, M.Y.; ur Rehman, E.; Ullah, S.; Atif, M.; Tariq, A. A review on laser cladding of high-entropy alloys, their recent trends and potential applications. *Manuf. Process.* **2021**, *68*, 225–273. [CrossRef]
114. Zhang, Q.; Zhang, F.; Liu, X.; Yue, Z.; Chen, X.; Wan, Z. Doping of laser-induced graphene and its applications. *Adv. Mater. Technol.* **2023**, *8*, 2300244. [CrossRef]
115. Zhang, Y.; Ding, G.; Kai, D.; Xie, X.; Zhang, F.; Zeng, Y.; Liu, G.; Wu, H.; Nie, Z. Nitrogen-doped graphene quantum dots for femtosecond ultrafast pulsed fiber lasers. *Opt. Fiber Technol.* **2023**, *80*, 103433. [CrossRef]
116. Liu, J.; Xu, J.; Cui, H.; Sun, X.; Mao, S.; Miao, Y.; Yu, J.; Han, J.; Kong, Z.Z.; Yang, T.; et al. Formation of highly-activated N-type shallow junction in germanium using nanosecond laser annealing and fluorine co-doping. *ECS J. Solid State Sci. Technol.* **2023**, *12*, 054002. [CrossRef]
117. Yasunami, T.; Nakamura, D.; Katayama, K.; Kakimoto, Y.; Kikuchi, T.; Ikenoue, H. Laser doping mechanism of 4H-SiC by KrF excimer laser irradiation using SiNx thin films. *Jpn. J. Appl. Phys.* **2023**, *62*, SC1039. [CrossRef]
118. Chery, N.; Zhang, M.; Monflier, R.; Mallet, N.; Seine, G.; Paillard, V.; Poumirol, J.M.; Larrieu, G.; Royet, A.S.; Kerdilès, S.; et al. Study of recrystallization and activation processes in thin and highly doped silicon-on-insulator layers by nanosecond laser thermal annealing. *J. Appl. Phys.* **2022**, *131*, 065301. [CrossRef]
119. Huet, K.; Aubin, J.; Raynal, P.-E.; Curvers, B.; Verstraete, A.; Lespinasse, B.; Mazzamuto, F.; Sciuto, A.; Lombardo, S.F.; La Magna, A.; et al. Pulsed laser annealing for advanced technology nodes: Modeling and calibration. *Appl. Surf. Sci.* **2020**, *505*, 144470. [CrossRef]
120. Al-Asedy, H.J.; Al-khafaji, S.A.; Ghoshal, S.K. Optical and electrical correlation effects in ZnO nanostructures: Role of pulsed laser annealing. *Opt. Mater.* **2021**, *115*, 111028. [CrossRef]
121. Taiwo, R.A.; Son, Y.; Shin, J. Evaluating suitability of green laser annealing in developing phosphorous-doped silicon for semiconductor devices. *Mater. Sci. Semicond. Process.* **2023**, *168*, 107865. [CrossRef]
122. Acosta Alba, P.; Aubin, J.; Perrot, S.; Mazzamuto, F.; Grenier, A.; Kerdilès, S. Solid phase recrystallization induced by multi-pulse nanosecond laser annealing. *Appl. Surf. Sci. Adv.* **2021**, *3*, 100053. [CrossRef]
123. Mulko, L.; Soldera, M.; Lasagni, A.F. Structuring and functionalization of non-metallic materials using direct laser interference patterning: A review. *Nanophotonics* **2022**, *11*, 203–240. [CrossRef]
124. Heffner, H.; Soldera, M.; Lasagni, A.F. Optoelectronic performance of indium tin oxide thin films structured by sub-picosecond direct laser interference patterning. *Sci. Rep.* **2023**, *13*, 9798. [CrossRef] [PubMed]
125. Lasagni, A.F.; Alamri, S.; Rößler, F.; Lang, V.; Voisiat, B. Design of Perfectly Ordered Periodic Structures on Polymers Using Direct Laser Interference Patterning. In *Wrinkled Polymer Surfaces*; González-Henríquez, C.M., Rodríguez-Hernández, J., Eds.; Springer International Publishing: Cham, Switzerland, 2019; pp. 157–180.
126. Mulko, L.; Wang, W.; Baumann, R.; Kress, J.; Voisiat, B.; Jaeger, E.; Leupolt, B.; Vaynzof, Y.; Soldera, M.; Lasagni, A.F. Understanding the relation between pulse duration and topography evolution of polyether ether ketones textures by ultrashort infrared laser interference patterning. *Adv. Funct. Mater.* **2022**, *24*, 2200688. [CrossRef]
127. Schütz, S.; Suarez, S.; Mücklich, F. Tribo-electric analysis of multi-cycle wear in asymmetric laser-structured Cu-Sn connectors. *Tribol. Lett.* **2023**, *71*, 127. [CrossRef]
128. Sikora, A.; Faucon, M.; Mincuzzi, G.; Kling, R. Fabrication of multisymmetrical hierarchical structures by direct laser interference patterning with 2 beams. *Appl. Surf. Sci.* **2023**, *638*, 158086. [CrossRef]
129. Liu, Y.-H.; Kuo, K.-K.; Cheng, C.-W.; Lee, A.-C. Femtosecond laser two-beam interference applied to 4H-SiC surface hierarchical micro-nano structure fabrication. *Opt. Laser Technol.* **2022**, *151*, 108081. [CrossRef]
130. Fox, T.; Maria Delfino, P.; Cortés, F.; Pauly, C.; Wyn Müller, D.; Briesenick, M.; Kickelbick, G.; Mücklich, F. Single-step production of photocatalytic surfaces via direct laser interference patterning of titanium. *ChemNanoMat* **2023**, *9*, e202300314. [CrossRef]
131. El-Khoury, M.; Voisiat, B.; Kunze, T.; Lasagni, A.F. Utilizing fundamental beam-mode shaping technique for top-hat laser intensities in direct laser interference patterning. *J. Laser Micro/Nanoeng.* **2018**, *13*, 268–272.
132. El-Khoury, M.; Voisiat, B.; Kunze, T.; Lasagni, A.F. Utilizing a diffractive focus beam shaper to enhance pattern uniformity and process throughput during direct laser interference patterning. *Materials* **2022**, *15*, 591. [CrossRef]
133. Lasagni, A.F.; Mulko, L.; Soldera, M. Ultrarapid Industrial Large-Area Processing Using Laser Interference Patterning Methods. In *Ultrafast Laser Nanostructuring: The Pursuit of Extreme Scales*; Springer Series in Optical Sciences; Stoian, R., Bonse, J., Eds.; Springer International Publishing: Cham, Switzerland, 2023; Volume 239, pp. 951–977.
134. Lasagni, A.F. How laser-based fabrication methods can be used to produce multifunctional surfaces. *Proc. SPIE* **2022**, *11988*, 1198802.

135. Shinde, S.; Mane, R.; Vardikar, A.; Dhumal, A.; Rajput, A. 4D printing: From emergence to innovation over 3D printing. *Eur. Polym. J.* **2023**, *197*, 112356. [CrossRef]
136. Ren, L.; Wang, Z.; Ren, L.; Xu, C.; Li, B.; Shi, Y.; Liu, Q. Understanding the role of process parameters in 4D printing: A review. *Compos. B. Eng.* **2023**, *265*, 110938. [CrossRef]
137. Ferretto, I.; Kim, D.; Lee, W.J.; Hosseini, E.; della Ventura, N.M.; Sharma, A.; Sofras, C.; Capek, J.; Polatidis, E.; Leinenbach, C. Shape memory and mechanical properties of a Fe-Mn-Si-based shape memory alloy: Effect of crystallographic texture generated during additive manufacturing. *Mater. Des.* **2023**, *229*, 111928. [CrossRef]
138. Tariq, A.; Arif, Z.U.; Khalid, M.Y.; Hossain, M.; Rasool, P.I.; Umer, R.; Ramakrishna, S. Recent advances in the additive manufacturing of stimuli-responsive soft polymers. *Adv. Eng. Mater.* **2023**, *25*, 2301074. [CrossRef]
139. Thakur, V.; Singh, R.; Kumar, R.; Gehlot, A. 4D printing of thermoresponsive materials: A state-of-the-art review and prospective applications. *Int. J. Interact. Des. Manuf.* **2023**, *17*, 2075–2094. [CrossRef]
140. Zhao, W.; Yue, C.; Liu, L.; Liu, Y.; Leng, J. Research progress of shape memory polymer and 4d printing in biomedical application. *Adv. Healthc. Mater.* **2023**, *12*, 2201975. [CrossRef] [PubMed]
141. Wang, X.; He, Y.; Liu, Y.; Leng, J. Advances in shape memory polymers: Remote actuation, multi-stimuli control, 4D printing and prospective applications. *Mater. Sci. Eng. R Rep.* **2022**, *151*, 100702. [CrossRef]
142. Alsaadi, M.; Hinchy, E.P.; McCarthy, C.T.; Moritz, V.F.; Zhuo, S.; Fuenmayor, E.; Devine, D.M. Liquid-based 4D printing of shape memory nanocomposites: A review. *J. Manuf. Mater. Process.* **2023**, *7*, 35. [CrossRef]
143. Wang, L.L.; Zhang, F.H.; Du, S.Y.; Leng, J.S. Advances in 4D printed shape memory composites and structures: Actuation and application. *Sci. China Technol. Sci.* **2023**, *66*, 1271–1288. [CrossRef]
144. Nugroho, W.T.; Dong, Y.; Pramanik, A.; Leng, J.; Ramakrishna, S. Smart polyurethane composites for 3D or 4D printing: General-purpose use, sustainability and shape memory effect. *Compos. B Eng.* **2021**, *223*, 109104. [CrossRef]
145. Alshahrani, H.A. Review of 4D printing materials and reinforced composites: Behaviors, applications and challenges. *J. Sci.: Adv. Mater. Devices* **2021**, *6*, 167–185. [CrossRef]
146. Liu, G.; Zhang, X.; Lu, X.; Zhao, Y.; Zhou, Z.; Xu, J.; Yin, J.; Tang, T.; Wang, P.; Yi, S.; et al. 4D additive–subtractive manufacturing of shape memory ceramics. *Adv. Mater.* **2023**, *35*, 2302108. [CrossRef] [PubMed]
147. Wan, L.; Mao, Z.; Liu, H.; Xie, Y.; Lyu, F.; Cao, Z.; He, Y.; Yin, J.; Han, X.; Chan, W.Y.K.; et al. Direct 4D printing of gradient structure of ceramics. *Chem. Eng. J.* **2023**, *465*, 142804. [CrossRef]
148. Wang, F.; Liu, C.; Yang, H.; Wang, H.; Zhang, H.; Zeng, X.; Wang, C.; Zhang, W.; Lv, W.; Zhu, P.; et al. 4D printing of ceramic structures. *Addit. Manuf.* **2023**, *63*, 103411. [CrossRef]
149. Huang, X.; Kang, N.; Coddet, P.; El Mansori, M. Analyses of the sliding wear behavior of NiTi shape memory alloys fabricated by laser powder bed fusion based on orthogonal experiments. *Wear* **2023**, *534–535*, 205130. [CrossRef]
150. Wei, S.; Zhang, J.; Zhang, L.; Zhang, Y.; Song, B.; Wang, X.; Fan, J.; Liu, Q.; Shi, Y. Laser powder bed fusion additive manufacturing of NiTi shape memory alloys: A review. *Int. J. Extrem. Manuf.* **2023**, *5*, 032001. [CrossRef]
151. Sreesha, R.B.; Ladakhan, S.H.; Mudakavi, D.; Adinarayanappa, S.M. An experimental investigation on performance of NiTi-based shape memory alloy 4D printed actuators for bending application. *Int. J. Adv. Manuf. Technol.* **2022**, *122*, 4421–4436. [CrossRef]
152. Babacan, N.; Pilz, S.; Hufenbach, J.; Gustmann, T. Effects of remelting on the properties of a superelastic Cu–Al–Mn shape memory alloy fabricated by laser powder bed fusion. *Shape Mem. Superelasticity* **2023**, *9*, 447–459. [CrossRef]
153. Seyedmohammadi, S.V.; Yapici, G.G. Effect of processing parameters on the phase transformation of a high temperature copper-based shape memory alloy. *J. Mater. Eng. Perform.* **2023**, *32*, 9440–9447. [CrossRef]
154. Ferretto, I.; Borzì, A.; Kim, D.; Della Ventura, N.M.; Hosseini, E.; Lee, W.J.; Leinenbach, C. Control of microstructure and shape memory properties of a Fe-Mn-Si-based shape memory alloy during laser powder bed fusion. *Addit Manuf. Lett.* **2022**, *3*, 100091. [CrossRef]
155. Mohri, M.; Ferretto, I.; Khodaverdi, H.; Leinenbach, C.; Ghafoori, E. Influence of thermomechanical treatment on the shape memory effect and pseudoelasticity behavior of conventional and additive manufactured Fe–Mn–Si–Cr–Ni-(V,C) shape memory alloys. *J. Mater. Res. Technol.* **2023**, *24*, 5922–5933. [CrossRef]
156. Yang, X.; Cheng, L.; Peng, H.; Qian, B.; Yang, L.; Shi, Y.; Chen, A.; Zhang, Z.; Zhao, L.; Hu, N.; et al. Development of Fe-Mn-Si-Cr-Ni shape memory alloy with ultrahigh mechanical properties and large recovery strain by laser powder bed fusion. *J. Mater. Sci. Technol.* **2023**, *150*, 201–216. [CrossRef]
157. Jafarabadi, A.; Ferretto, I.; Mohri, M.; Leinenbach, C.; Ghafoori, E. 4D printing of recoverable buckling-induced architected iron-based shape memory alloys. *Mater. Des.* **2023**, *233*, 112216. [CrossRef]
158. Abedi, H.; Algamal, A.; Abdollahzadeh, M.; Nematollahi, M.; Alafaghani, A.; Bayati, P.; Elahinia, M.; Qattawi, A. Predicting transformation temperatures of additively manufactured NiTiHf shape memory alloy using neural network modeling. *JOM* **2023**, *75*, 4515–4525. [CrossRef]
159. Milleret, A. 4D printing of Ni–Mn–Ga magnetic shape memory alloys: A review. *Mater. Sci. Technol.* **2022**, *38*, 593–606. [CrossRef]
160. Zhang, Q.; Zhao, Z.; Wu, D.; Chen, K.; Weng, S. Mechanics-guided design of inflatable heterogeneous shape memory polymer vascular stents. *Int. J. Mech. Sci.* **2023**, *254*, 108405. [CrossRef]
161. Jeewantha, L.H.J.; Epaarachchi, J.A.; Forster, E.; Islam, M.; Leng, J. Early research of shape memory polymer vascular stents. *Express Polym. Lett.* **2022**, *16*, 902–923. [CrossRef]

162. Costanza, G.; Tata, M.E. Shape memory alloys for aerospace, recent developments, and new applications: A short review. *Materials* **2020**, *13*, 1856. [CrossRef]
163. Oh, H.-U.; Kim, H.-I.; Kim, J.-K.; Choi, J.-S.; Kim, S.-H. Smartphone CanSat for actualization of real-time streaming video calls using remote screen touch system with shape memory alloy actuator. *Trans. Jpn. Soc. Aeronaut. Space Sci.* **2019**, *62*, 256–264. [CrossRef]
164. Battaglia, M.; Sellitto, A.; Giamundo, A.; Visone, M.; Riccio, A. Shape memory alloys applied to automotive adaptive aerodynamics. *Materials* **2023**, *16*, 4832. [CrossRef]
165. Shreekrishna, S.; Nachimuthu, R.; Nair, V.S. A review on shape memory alloys and their prominence in automotive technology. *J. Intell. Mater. Syst. Struct.* **2023**, *34*, 499–524. [CrossRef]
166. Cristiano, F.; La Magna, A. (Eds.) *Laser Annealing Processes in Semiconductor Technology: Theory, Modeling and Applications in Nanoelectronics*; Woodhead Publishing: Sawston, UK; Elsevier Ltd., Elsevier Science et Technology: San Diego, CA, USA, 2021; 410p.
167. Matos, R.; Pala, N. A Review of phase-change materials and their potential for reconfigurable intelligent surfaces. *Micromachines* **2023**, *14*, 1259. [CrossRef] [PubMed]
168. Wang, Y.; Ning, J.; Lu, L.; Bosman, M.; Simpson, R.E. A scheme for simulating multi-level phase change photonics materials. *NPJ Comput. Mater.* **2021**, *7*, 183. [CrossRef]
169. Kunkel, T.; Vorobyov, Y.; Smayev, M.; Lazarenko, P.; Kolobov, A.; Kozyukhin, S. Self-organized structures in thin films of phase-change material upon femtosecond laser excitation: From periodic ordering to ablation. *Appl. Surf. Sci.* **2023**, *624*, 157122. [CrossRef]
170. Torun, G.; Yadav, A.; Richardson, K.A.; Bellouard, Y. Ultrafast laser direct-writing of self-organized microstructures in Ge-Sb-S chalcogenide glass. *Front. Phys.* **2022**, *10*, 883319. [CrossRef]
171. D'amico, C.; Martin, G.; Troles, J.; Cheng, G.; Stoian, R. Multiscale laser written photonic structures in bulk chalcogenide glasses for infrared light transport and extraction. *Photonics* **2021**, *8*, 211. [CrossRef]
172. Pan, L.; Song, B.; Mao, N.; Xiao, C.; Lin, C.; Zhang, P.; Shen, X.; Dai, S. Optical properties of Ge-Sb-Se thin films induced by femtosecond laser. *Opt. Commun.* **2021**, *496*, 127123. [CrossRef]
173. Somayaji, M.; D'Amico, C.; Wu, Y.; Troles, J.; Stoian, R. Influence of thermal annealing on ultrafast laser-induced local densification in bulk sulfur-based chalcogenide glasses. *Phys. Status Solidi A* **2019**, *216*, 1800568. [CrossRef]
174. Wang, X.; Qi, H.; Hu, X.; Yu, Z.; Ding, S.; Du, Z.; Gong, Q. Advances in photonic devices based on optical phase-change materials. *Molecules* **2021**, *26*, 2813. [CrossRef]
175. Sahoo, D.; Naik, R. GSST phase change materials and its utilization in optoelectronic devices: A review. *Mater. Res. Bull.* **2022**, *148*, 111679. [CrossRef]
176. Sahoo, D.; Naik, R. A review on the linear/nonlinear optical properties of Se doped chalcogenide thin films as potential optoelectronic applications. *J. Non-Cryst. Solids* **2022**, *597*, 121934. [CrossRef]
177. Wang, X.; Yu, H.; Li, P.; Zhang, Y.; Wen, Y.; Qiu, Y.; Liu, Z.; Li, Y.; Liu, L. Femtosecond laser-based processing methods and their applications in optical device manufacturing: A review. *Opt. Laser Technol.* **2021**, *135*, 106687. [CrossRef]
178. Belousov, D.A.; Kuts, R.I.; Okotrub, K.A.; Korolkov, V.P. Direct laser writing of diffractive structures on Bi-layer Si/Ti films coated on fused silica substrates. *Photonics* **2023**, *10*, 771. [CrossRef]
179. Peng, M.; Lu, Z.; Tang, Y.; Li, C.; Ren, J.; Dong, C.; Liu, C. Femtosecond laser direct writing of long period fiber grating sensor with high refractive index sensitivity. *Opt. Fiber Technol.* **2023**, *81*, 103511. [CrossRef]
180. Shakhno, E.A.; Nguyen, Q.D.; Sinev, D.A.; Veiko, V.P. Lateral proximity effect in direct laser thermochemical recording on thin titanium films. *Opt. Quantum Electron.* **2023**, *55*, 502. [CrossRef]
181. Cheng, Z.; Cao, R.; Wei, K.; Yao, Y.; Liu, X.; Kang, J.; Dong, J.; Shi, Z.; Zhang, H.; Zhang, X. 2D materials enabled next-generation integrated optoelectronics: From fabrication to applications. *Adv. Sci.* **2021**, *8*, 2003834. [CrossRef] [PubMed]
182. Zhang, J.; Zhang, T.; Zhang, H.; Wang, Z.; Li, C.; Wang, Z.; Li, K.; Huang, X.; Chen, M.; Chen, Z.; et al. Single-crystal SnSe thermoelectric fibers via laser-induced directional crystallization: From 1D fibers to multidimensional fabrics. *Adv. Mater.* **2020**, *32*, 2002702. [CrossRef] [PubMed]
183. Kamanina, N. Refractive properties of conjugated organic materials doped with fullerenes and other carbon-based nano-objects. *Polymers* **2023**, *15*, 2819. [CrossRef] [PubMed]
184. Wieszczycka, K.; Staszak, K.; Woźniak-Budych, M.J.; Litowczenko, J.; Maciejewska, B.M.; Jurga, S. Surface functionalization—The way for advanced applications of smart materials. *Coord. Chem. Rev.* **2021**, *436*, 213846. [CrossRef]
185. Pallarés-Aldeiturriaga, D.; Roldán-Varona, P.; Rodríguez-Cobo, L.; López-Higuera, J.M. Optical fiber sensors by direct laser processing: A review. *Sensors* **2020**, *20*, 6971. [CrossRef]
186. Shin, J.H.; Kim, Y.B.; Park, J.H.; Lee, J.S.; Park, S.H.; Lee, S.H.; Lee, J.H.; Lee, K.J. Light-material interfaces for self-powered optoelectronics. *J. Mater. Chem. A* **2021**, *9*, 25694–25705. [CrossRef]
187. Wu, C.; Yu, H. Programmable phase-change metasurfaces on waveguides for multimode photonic convolutional neural network. *Nat. Commun.* **2021**, *12*, 96. [CrossRef]
188. Kathryn, E. Optimizing laser optics for green energy applications. *J. Lasers Opt. Photonics* **2023**, *10*, 93.
189. Antolini, F.; Orazi, L. Quantum dots synthesis through direct laser patterning: A review. *Front. Chem.* **2019**, *7*, 252. [CrossRef] [PubMed]

190. Zhao, J.; Zhao, Y.; Peng, Y.; Lv, R.-Q.; Zhao, Q. Review of femtosecond laser direct writing fiber-optic structures based on refractive index modification and their applications. *Opt. Laser Technol.* **2022**, *146*, 107473. [CrossRef]
191. Song, S.; Lonsethagen, K.; Laurell, F.; Hawkins, T.W.; Ballato, J.; Fokine, M.; Gibson, U.J. Laser restructuring and photoluminescence of glass-clad GaSb/Si-core optical fibres. *Nat. Commun.* **2019**, *10*, 1790. [CrossRef] [PubMed]
192. Mühlberger, K.; Harvey, C.M.; Fokine, M. Temperature dynamics in silicon core fibers during CO_2 laser processing. *Opt. Express* **2022**, *30*, 92–100. [CrossRef]
193. Zaengle, T.; Martinez, E.; Hawkins, T.W.; McMillen, C.; Ballato, J. A novel route to fibers with volatile crystalline semiconductor cores Part 2: Selenides and phosphides. *Opt. Mater.* **2023**, *145*, 114388. [CrossRef]
194. Zaengle, T.; Gibson, U.J.; Hawkins, T.W.; McMillen, C.; Ghimire, B.; Rao, A.M.; Ballato, J. A novel route to fibers with incongruent and volatile crystalline semiconductor cores: GaAs. *ACS Photonics* **2022**, *9*, 1058–1064. [CrossRef]
195. Han, B.; Luo, Q.; Zhang, P.; Zhang, T.; Tang, G.; Chen, Z.; Zhang, H.; Zhong, B.; Zeng, Y.; Sun, M.; et al. Multifunctional single-crystal tellurium core multimaterial fiber via thermal drawing and laser recrystallization. *J. Am. Ceram. Soc.* **2022**, *105*, 1640–1647. [CrossRef]
196. Jaiswal, A.; Rastogi, C.K.; Rani, S.; Singh, G.P.; Saxena, S.; Shukla, S. Two decades of two-photon lithography: Materials science perspective for additive manufacturing of 2D/3D nano-microstructures. *iScience* **2023**, *26*, 106374. [CrossRef]
197. Rahman, A.; Mariotto, G.; Cattaruzza, E.; Trave, E.; Gonella, F.; Quaranta, A. Thermal annealing and laser-induced mechanisms in controlling the size and size-distribution of silver nanoparticles in Ag+-Na+ ion-exchanged silicate glasses. *J. Non-Cryst. Solids* **2021**, *563*, 120815. [CrossRef]
198. Doskolovich, L.L.; Mingazov, A.A.; Byzov, E.V.; Skidanov, R.V.; Ganchevskaya, S.V.; Bykov, D.A.; Bezus, E.A.; Podlipnov, V.V.; Porfirev, A.P.; Kazanskiy, N.L. Hybrid design of diffractive optical elements for optical beam shaping. *Opt. Express* **2021**, *29*, 31875–31890. [CrossRef] [PubMed]
199. Kazanskiy, N.L.; Khonina, S.N.; Karpeev, S.V.; Porfirev, A.P. Diffractive optical elements for multiplexing structured laser beams. *Quantum Electron.* **2020**, *50*, 629–635. [CrossRef]
200. Doskolovich, L.L.; Skidanov, R.V.; Bezus, E.A.; Ganchevskaya, S.V.; Bykov, D.A.; Kazanskiy, N.L. Design of diffractive lenses operating at several wavelengths. *Opt. Express* **2020**, *28*, 11705–11720. [CrossRef] [PubMed]
201. Siemion, A. The Magic of Optics—An Overview of Recent Advanced Terahertz Diffractive Optical Elements. *Sensors* **2021**, *21*, 100. [CrossRef] [PubMed]
202. Murzin, S.P.; Bielak, R.; Liedl, G. Algorithm for calculating of the power density distribution of the laser beam to create a desired thermal effect on technological objects. *Comput. Opt.* **2016**, *40*, 679–684. [CrossRef]
203. Murzin, S.P. Local laser annealing for aluminium alloy parts. *Lasers Eng.* **2016**, *33*, 67–76.
204. Murzin, S.P.; Kazanskiy, N.L. Arrays formation of zinc oxide nano-objects with varying morphology for sensor applications. *Sensors* **2020**, *20*, 5575. [CrossRef]
205. Kudryashov, S.I.; Danilov, P.A.; Porfirev, A.P.; Saraeva, I.N.; Nguyen, T.H.T.; Rudenko, A.A.; Khmelnitskii, R.A.; Zayarny, D.A.; Ionin, A.A.; Kuchmizhak, A.A.; et al. High-Throughput Micropatterning of Plasmonic Surfaces by Multiplexed Femtosecond Laser Pulses for Advanced IR-Sensing Applications. *Appl. Surf. Sci.* **2019**, *484*, 948–956. [CrossRef]
206. Murzin, S.P. Laser irradiation for enhancing mass transfer in the solid phase of metallic materials. *Metals* **2021**, *11*, 1359. [CrossRef]
207. Murzin, S.P. Formation of ZnO/CuO heterostructures based on quasi-one-dimensional nanomaterials. *Appl. Sci.* **2023**, *13*, 488. [CrossRef]
208. Murzin, S.P.; Kazanskiy, N.L. Creation of one- and two-dimensional copper and zinc oxides semiconductor structures. *Appl. Sci.* **2023**, *13*, 11459. [CrossRef]
209. Murzin, S.P.; Balyakin, V.B.; Gachot, C.; Fomchenkov, S.A.; Blokhin, M.V.; Kazanskiy, N.L. Ultraviolet nanosecond laser treatment to reduce the friction coefficient of silicon carbide ceramics. *Appl. Sci.* **2021**, *11*, 11906. [CrossRef]
210. Katz, S.; Kaplan, N.; Grossinger, I. Using diffractive optical elements-does for beam shaping—Fundamentals and applications. *Opt. Photonik* **2018**, *13*, 83–86. [CrossRef]
211. Danilov, V.A. Laser technology and nanotechnology applying diffractive optical elements. *Nanobiotechnology Rep.* **2022**, *17*, 747–757. [CrossRef]